

The Importance of Factorial Design of Experiments in Functional Nanomaterials Preparation and Performance



Alexandre H. Pinto

Abstract The experimental planning and design are important parts for successful performance and result analysis in a project. Both for industry and academic settings, there is the constant need to analyze the influence of many variables in the different types of responses. Traditionally, the influence of different variables in the experimental outcome has been analyzed by changing “one factor at a time”, which is usually described as univariate or OFAT approach. However, unless all variables are close to their optimum value, there is no guarantee that this approach will lead to the best optimized outcome. Additionally, the OFAT approach can lead to the implementation of an excessive number of experiments, which usually increases the expenses related to the project. Pursuing to analyze how the synergy between different variables can influence the experimental outcomes, there is the multivariate approach, where two or more variables are changed simultaneously enabling the experimentalist to analyze the beneficial or antagonistic effect of this combination of variables in the experimental outcome. Moreover, the multivariate approach may improve the chances to find the best outcome possible with the conduction of a fewer number of experiments. In this sense, this chapter introduces the concept of factorial design of experiments, a multivariate approach based on choosing two or more levels for multiple variables, calculating the effects of each variable individually and of each possible combination of variables, obtaining a model from these results, applying this model to predict untested conditions and judge the statistic significance of the model. The examples presented in the chapter will all be focused on the preparation and performance of nanomaterials. For instance, how the concentrations of different precursors can influence the particle size of colloidal silica nanoparticles. Or how different variables, such as, time, temperature and reagents concentration can influence the thickness of manganese sulfide (MnS) thin films. The chapter begins providing the definition of the basic terms underlying the factorial design, then, it presents examples from literature applying factorial designs starting with the simpler ones, such as 2^3 . Then, the chapter evolves presenting optimization and

A. H. Pinto (✉)

Department of Chemistry and Biochemistry, Manhattan College, 4513 Manhattan College Parkway, Riverdale, NY 10471, USA

e-mail: alex.pinto@manhattan.edu

© The Author(s), under exclusive license to Springer Nature Switzerland AG 2021

387

F. A. La Porta and C. A. Taft (eds.), *Functional Properties of Advanced*

Engineering Materials and Biomolecules, Engineering Materials,

https://doi.org/10.1007/978-3-030-62226-8_14

response surface methodologies factorial designs, for instance, central composite, Box-Behken, and Doehlert designs. Finally, the chapter presents tables with references from papers published in the period from 2015 to 2020. In each one of them, the factorial design of experiments was used for the development of functional materials applied in nanoparticles preparation, drug delivery and encapsulation, wastewater remediation, and solar cells development. With this chapter, the author hopes to introduce a powerful and underexplored statistical tool to scientists, engineers, and all practitioners of nanomaterials science. Focus will be placed on how they can benefit from the concepts and examples presented, and possibly adapt them for their own projects, instead of relying on heavy mathematical notations and calculations.

1 Introduction

The development of functional materials requires accurate control of each step in their production. In this sense, to be able to test a broader range of experimental conditions by performing a lower number of experiments is desirable. So, the factorial design of experiments is a set of statistical concepts intended to optimize specific properties by taking advantage of a multivariate approach. In this approach, the interaction between different factors is interpreted holistically. The design of experiments allows the research to judge which factors are statistically significant by calculating their effects on the property to be optimized. Moreover, empirical models can be obtained, allowing the researcher to predict how that specific property will behave in untested conditions.

The ability to predict results based on an empirical model opens up an array of opportunities and saves time and resources from the researcher. So, this chapter aims to show from the scientific literature examples how the factorial design of experiments has widely been applied to the development and performance of functional materials.

This chapter is intended to fulfill the needs of readers with different knowledge levels about the design of experiments, from the beginner to the experienced reader.

That being said, readers from different familiarity levels have the opportunity to focus their attention on different parts of the chapter. For the beginner ones, it is recommended to start reading the chapter from Sect. 2. Since in this part, the essential concepts and terminology of factorial design are introduced. Then, a step by step 2^3 factorial design is performed. This 2^3 factorial design is developed very comprehensively, aiming that even a beginner reader can try to adapt the design to their own experimental situation, without using black-box programs. This part appreciates the statistical formalism whenever it is necessary. In such a way, it can sound intimidating at first sight. However, with attention and persistence, the reader can benefit from the knowledge.

Since Sect. 2 is very comprehensive. Consequently, it is also extensive. So, if a reader is already familiar with all the terminology, structure, and calculations related to factorial designs, he/she is welcome to skip this full part and start straight on Sect. 3. There, the reader will find analyses of literature examples where the factorial design

of experiments and response surface methodologies were applied to the context of materials preparation and performance. This part appreciates a critical analysis of each research paper by remarking the steps followed by the authors.

Finally, in Sect. 4, readers will find references from papers published in the period from 2015 to 2020. In each one of them, the factorial design of experiments was applied to the development of four types of functional materials. They are nanoparticles preparation, drug encapsulation and delivery, wastewater remediation, and solar cell development.

2 The Fundamentals and Statistical Basis of the Factorial Design of Experiments

2.1 Factorial Design of Experiments: Initial Concepts and Terminology

The experimental planning and design are essential parts for successful performance and analysis of results in a project. Both for industry and academic settings, there is a constant need to analyze the influence of many factors in the different types of responses. Traditionally, the impact of different factors in the experimental outcome has been analyzed by changing “one factor at a time,” which is usually described as a univariate or OFAT approach.

For instance, suppose that a research group is aiming to maximize the yield of a certain chemical reaction, and they know that the yield can be affected by factors such as pH, temperature, and catalyst concentration. From previous literature knowledge, the scientists figured out that this reaction has been described to occur in the following ranges for each factor, as presented in Table 1.

According to the OFAT approach, they would perform a series of experiments varying the pH and keeping temperature and catalyst concentration constant. For instance, by fixing the temperature at 85 °C, the catalyst concentration at 5×10^{-4} mol L⁻¹, and making the pH equal to 8, 10, 12, and 14 units.

Next, they would vary the temperature and keep the pH and catalyst concentration constant. For instance, by fixing pH equal to 14, catalyst concentration at 5×10^{-4} mol L⁻¹, and making the temperature equal to 25, 50, 70, and 85 °C.

Then, they would vary catalyst concentration and keep pH and temperature constant. For instance, by fixing pH equal to 14, temperature at 85 °C, and making

Table 1 Matrix of experiments showing the factors and their respective lower and upper limits

Factor	Lower limit	Upper limit
pH	8	14
Temperature (°C)	25	85
Catalyst concentration (mol L ⁻¹)	1×10^{-4}	5×10^{-4}

catalyst concentration equal to 1×10^{-4} , 2.5×10^{-4} , 3.5×10^{-4} , and 5×10^{-4} mol L⁻¹.

There are potential flaws associated with this OFAT approach. The first one is related to choosing the values for the factors that will remain fixed [1]. Notice that, whenever fixing the pH and catalyst concentration, the researchers always chose to fix them at the uppermost level possible. This choice could have been determined by a preconceived idea that maximizing factor values always are going to lead to a yield maximization, which is not always true.

Second, this OFAT approach could ignore potential effects related to the interaction of two or more factors being varied at the same time [1]. For instance, the yield could be maximized at pH 11, 30 °C, and catalyst concentration equal to 1.5×10^{-4} mol L⁻¹. This condition was not performed in the OFAT approach adopted, so the researchers would not be aware of the yield maximization at this set of conditions.

A third potential flaw could be related to the large number of experiments performed [1]. In general, a higher number of experiments represent higher consumption of chemicals, analysis time, production of waste, and, consequently, a higher total cost. In this sense, an approach that offers useful trends and conclusions with a lower amount of experiments is always preferred. So, in the next section, we will see how this experimental approach could be redesigned according to the factorial design of experiments. And how the factorial design could potentially decrease the chance of each of these flaws to occur.

2.2 *Planning According to the Factorial Design of Experiments*

Pursuing to analyze how the interaction between different variables can influence the experimental outcomes, there is the multivariate approach. Where two or more variables are changed simultaneously, enabling the researcher to analyze the beneficial or antagonistic effect of this interaction of variables in the experimental outcome. Moreover, the multivariate approach may improve the chances to find the best result possible with the conduction of a fewer number of experiments.

Before we start redesigning the series of experiments shown in the previous section, we should define the terms commonly related to the factorial design of experiments. The first term is **factor**. Factors, as seen in the previous section, are the variables that would be varied across the experimental design. So, according to the situation we are analyzing, three factors have been studied, they are pH, temperature, and catalyst concentration.

The second term is the **response variable**, which is the response the researchers are aiming to observe by performing the experiments. In the example presented, the yield is the response variable. It is important to say that experimental designs can have more than one response variable.

The values each factor will adopt will be called **levels**. For instance, let's suppose that the temperature will be fixed in their lowest and highest values, so, respectively, 25 and 85 °C. In this case, 25 and 85 °C are called the levels of the temperature factor. If only two levels are adopted for each factor, then the factorial design is called a **two-level factorial design**. Now, supposing that the scientist had chosen three levels for each variable, in that case, the factorial design would be called **three-level factorial design**. The levels could either be quantitative or qualitative. In case qualitative levels are chosen, it is necessary to consistently order them in such a way that a certain level is defined as the lower level, and the other one is the upper level, taking the two-level factorial design as an example.

The **effects** are how single factors or the interaction of two or more factors would influence the value obtained for the response variable. For instance, among the three factors studied, one of them, for instance, temperature, may have a higher influence on the response variable. Whereas, other factors may be concluded to be insignificant to change the response variable. The total number of possible effects will be dependent on how many factors the experimental design has.

In the studied example, as there are three factors, each factor will have its individual effect. Then, the design can have secondary effects, which will arise from the interaction of two factors at a time. So, the secondary factors would be pH-Temperature, pH-Catalyst Concentration, and Temperature-Catalyst Concentration. Finally, in models having three or more factors, tertiary effects are predicted, which are obtained by the combination of three variables at a time. In the studied example, the only tertiary effect would be pH-Temperature-Catalyst Concentration. If the design had four factors, it would have more tertiary effects and one quaternary effect. In conclusion, this three-factor, two-level experimental design has three primary effects, three secondary effects, and one tertiary effect.

A **factorial design** is the experimental design comprising all levels of each factor studied varied in a multivariate manner, in such a way that allows the interaction effects to be calculated. In general, the factorial designs are named according to how many factors they have and how many levels each factor has. A common representation for the factorial design name is s^k , where k is equal to the number of factors, and s is how many levels each factor has. In the studied example, which has three factors, and two levels for each one of them, this can be called to be a **2^3 factorial design**.

The s^k representation also indicates the minimum number of experiments without replicas to be performed to be considered a full s^k factorial design. To figure out the number of experiments it is necessary to solve the exponential equation shown in the s^k representation, for instance, a 2^3 factorial design would require a minimum of $2^3 = 8$ different experimental conditions to be considered complete.

Another important concept is the **coded levels**. For calculating the effects and their statistical significance, matrix calculations will be necessary. In this sense, each level, whether it is quantitative or qualitative, should be normalized according to a common scale. In general, this scale ranges from -1 to $+1$. In the case of two-level factorial design, the lower limit is normalized as -1 , and thus, the upper limit

Table 2 The factors with their respective limits represented as coded (in parenthesis) and uncoded values

Factor	Lower limit	Upper limit
pH = A	8 (-1)	14 (+1)
Temperature ($^{\circ}\text{C}$) = B	25 (1)	85 (+1)
Catalyst concentration (mol L^{-1}) = C	1×10^{-4} (-1)	5×10^{-4} (+1)

Table 3 Matrix of experiments

Exp. number	pH	Temperature	Catalyst concentration
1	-1	-1	-1
2	+1	-1	-1
3	-1	+1	-1
4	+1	+1	-1
5	-1	-1	+1
6	+1	-1	+1
7	-1	+1	+1
8	+1	+1	+1

is normalized as +1. So, Table 1 could be improved to include the coded values between parenthesis, as shown in Table 2.

Matrix of experiments is the matrix that describes each experiment to be performed, according to the combination of the coded values for each factor. For instance, for the example given, as shown in Table 3.

Translating the matrix of experiments from the coded values to the original values, one can say that the experiment number 1 is performed with pH = 8, Temperature = 25°C , and catalyst concentration = $1 \times 10^{-4} \text{ mol L}^{-1}$. Taking another example, experiment 7 is performed at pH = 8, Temperature = 85°C , and catalyst concentration = $5 \times 10^{-4} \text{ mol L}^{-1}$.

The **matrix of results** is the one that summarizes the values observed for the response variable for each one of the experiments performed, as shown in Table 4.

Table 4 Matrix of results

Exp. number	Yield (%)
1	25
2	42
3	76
4	45
5	81
6	5
7	66
8	15

After being introduced to the essential vocabulary and concepts about factorial design, we are ready to start seeing how the factorial design is structured.

2.3 *The Structure of the Factorial Design*

Factorial Design starts with its planning. In the **planning** stage, the factors and response variables to be studied should be defined. Then, within each factor is necessary to identify the upper and lower levels.

When planning a factorial design, it is essential to understand that there is no “one-size fits all” solution for all the scientific problems. However, there are some steps that the researcher can follow to better planning the design. For instance, the factors, their respective levels, and the response variables could be defined according to the need of the process that the researcher is aiming to optimize. Scientific or technical literature about the problem to be solved is a reasonable starting point. Also, the levels can be defined according to the capabilities of the pieces of equipment available for that experiment performance. The cost of using a specific piece of equipment or technique could be another decisive factor while planning the design [2].

In summary, to plan a factorial design accordingly, it is necessary: (a) to be familiar to the system to be studied, (b) to know the technical resources available, (c) to have clear goals about what is the response variable to be optimized, and (d) how the researcher is aiming to optimize this response variable, for instance, either maximizing or minimizing its value [3].

The second step in the factorial design is the **factor screening**. Due to the prior knowledge of the system, the researcher can identify variables that influence the response variable he/she is interested in optimizing. So, at this point, the researcher will perform a factor screening step. During factor screening, experiments will be performed according to some 2^k factorial design or some 2^{k-p} fractional factorial design. In either case, k is the number of factors to be studied. Then, all the experiments necessary to complete the selected factorial design will be performed. These experiments can be achieved with or without replicas, depending on the time and resources available to the researcher.

After the experiments conclusion, the researcher will analyze the data and determine which factors have significant effects and which factors do not have significant effects regarding influencing the response variable. At this point, the researcher will be able to obtain a linear polynomial equation describing how the significant factors quantitatively influence the response variable. For some situations, the model described by this equation can be enough to answer satisfactorily the question asked by the researcher. And the design can even be concluded on this point [3].

However, for other situations, the linear polynomial model obtained may not accurately describe the situation faced by the researcher. In this case, the factorial design will proceed to an **optimization** step. In this step, the insignificant factors will be disregarded, and additional experiments will be performed, considering only



Fig. 1 The four general steps of a factorial design of experiments

the significant factors. Also, in this step, in general, more than two levels will need to be considered for every factor [3, 4].

As more than two levels will be considered for each factor, the optimization step will allow the research to obtain a model described by a polynomial equation of order higher than one, for instance, a quadratic polynomial equation. Also, as the optimization is a refinement step, some factors may prove to be insignificant under the new design conditions. Consequently, they will be excluded from the definite model equation [4].

Most of the time, after one or a few optimization steps, the researcher will have a model that describes with satisfactory precision the behavior of the system in the study. Then, the next step is the **conclusion** of the design. In this step, the researcher will interpret how the empirical model obtained translates in the context of the studied situation. Additionally, the researcher will be able to apply the model to experimental conditions initially untested and verify how the experimental result agrees with the result predicted by the model.

The successful accomplishment of the four steps shown in Fig. 1 describes what is required to complete a factorial design. In the next two sections, we will discuss how the screening and optimization steps can be performed by using different types of factorial designs and their particularities.

2.4 Screening the Factors

Depending on the complexity of the experimental problem to be solved, many factors can influence the response variable. In this sense, it is necessary to have a screening step, which will start with most of the factors that can hypothetically change the response variable. Then, the significance of the effects of these factors will be judged according to appropriate statistical tests, and the insignificant factors will be excluded from the optimization step. Besides deciding the significance of the effects, another goal from the screening step is to obtain a first-order polynomial equation, describing how the response variable varies according to changing the coded values of the significant factors.

The main differences between 2^k and 2^{k-p} factorial designs are shown in Table 5, as adapted from Candiotti et al. [5].

The fractional factorial designs 2^{k-p} are beyond the scope of this chapter. For readers interested in learning more regarding this type of design, references number

Table 5 Comparison of the features of the full factorial design (2^k) and fractional factorial design (2^{k-p})

Design	Type of factors	Type of response variable	Number of factors	Minimum number of experiments	Number of estimated effects
2^k	Quantitative or qualitative	Quantitative	Usually between 2 and 5	2^k	$2^k - 1$
2^{k-p}	Quantitative or qualitative	Quantitative	Usually higher than 4	2^{k-p}	It depends on p value and how cofounded the design is

[3] and [6] are good references to learn the essential concepts of fractional factorial designs.

2.5 2^k Factorial Designs

In Sect. 2.2, we first defined what 2^k factorial designs are and how many experiments are necessary to complete the design according to the k value. A feature of a 2^k factorial design is that for each factor, only two levels are defined, a lower and an upper level. This feature holds for 2^k factorial designs used in the factors screening steps. For more comprehensive steps, like the ones used for optimization steps, more levels will be needed. In this section, we will see the particularities of a 2^k factorial design. For instance, we will discuss how to calculate the effects and the coefficients of the equation describing the design model, and how to judge the significance of these effects.

Before we start, it is important to say that to perform all the calculations and graphs presented in this section does not require any specialized software. Any software able to program matrix multiplication and graphical plotting, for instance, Microsoft Excel, is enough to perform all the calculations. However, there are software packets specialized to perform all of the design of experiments calculations, most of them are paid packages. The readers more interested to know the names and capabilities of these software packages are encouraged to read the review paper by Hibbert [7], which contains a table listing the main commercial softwares used in design of experiment calculations.

As shown in Table 6, the number of effects possible for a 2^k factorial design is equal to $2^k - 1$. In this sense, Table 6 explains how many and which are the effects, according to the k value.

Each one of the effects can be calculated according to the Eq. 1, as exemplified for Effect A [8]:

Table 6 Number and type of effects according to the number of factors (k value) in a 2^k factorial design

k value	Factors	Number of effects	Primary effects	Interaction effects
2	A, B	3	A, B	AB
3	A, B, C	7	A, B, C	AB, AC, BC, ABC
4	A, B, C, D	15	A, B, C, D	AB, AC, AD, BC, BD, CD, ABC, ABD, ADC, BDC, ABCD

$$Effect_A = \frac{\sum Y_{(+)}^A}{n/2} - \frac{\sum Y_{(-)}^A}{n/2} \tag{1}$$

where $Y_{(+)}^A$ are the values of the response variable for which A has coded value = +1, $Y_{(-)}^A$ are the values of the response variable for which A has coded value = -1. n is defined as the total number of experiments in the factorial design, for instance, n = 8 for a 2³ or n = 16 for a 2⁴. Notice that the n value does not change if replicas are performed. The only thing that changes in case replicas were performed is the fact that each $Y_{(+)}^A$ and $Y_{(-)}^A$ should be taken as the average of the replicas.

A good way to understand the Eq. 1 is to think that the effect is the difference between the average of the response variable when A has coded value = +1 and the average of the response variable when A has coded value = -1.

To minimize the chances to be mistaken during the calculation of the effects, an alternative to Eq. 1, is to use matrix multiplication for each one of the effects. In Table 3, in Sect. 2.2, we introduced the concept of the matrix of experiments. Here, we will expand that matrix to include the coded values for each one of the possible interactions.

The coded value for each interaction was obtained by simply multiplying the coded values of the factors giving rise to that respective interaction. We can convert Table 7 in a square matrix (a matrix having the same number of columns and rows) by adding a column where all entries will be +1, as the first column of the matrix.

Table 7 Matrix of experiments for the primary effects and interactions in a 2³ factorial design

Exp. Number	A	B	C	AB	AC	BC	ABC
1	-1	-1	-1	+1	+1	+1	-1
2	+1	-1	-1	-1	-1	+1	+1
3	-1	+1	-1	-1	+1	-1	+1
4	+1	+1	-1	+1	-1	-1	-1
5	-1	-1	+1	+1	-1	-1	+1
6	+1	-1	+1	-1	+1	-1	-1
7	-1	+1	+1	-1	-1	+1	-1
8	+1	+1	+1	+1	+1	+1	+1

We can call this matrix as matrix (M1):

$$X = \begin{bmatrix} +1 & -1 & -1 & -1 & +1 & +1 & +1 & -1 \\ +1 & +1 & -1 & -1 & -1 & -1 & +1 & +1 \\ +1 & -1 & +1 & -1 & -1 & +1 & -1 & +1 \\ +1 & +1 & +1 & -1 & +1 & -1 & -1 & -1 \\ +1 & -1 & -1 & +1 & +1 & -1 & -1 & +1 \\ +1 & +1 & -1 & +1 & -1 & +1 & -1 & -1 \\ +1 & -1 & +1 & +1 & -1 & -1 & +1 & -1 \\ +1 & +1 & +1 & +1 & +1 & +1 & +1 & +1 \end{bmatrix} \quad (M1)$$

The transpose matrix (X^t) of the matrix 1 can be written as matrix (M2)

$$X^t = \begin{bmatrix} +1 & +1 & +1 & +1 & +1 & +1 & +1 & +1 \\ -1 & +1 & -1 & +1 & -1 & +1 & -1 & +1 \\ -1 & -1 & +1 & +1 & -1 & -1 & +1 & +1 \\ -1 & -1 & -1 & -1 & +1 & +1 & +1 & +1 \\ +1 & -1 & -1 & +1 & +1 & -1 & -1 & +1 \\ +1 & -1 & +1 & -1 & -1 & +1 & -1 & +1 \\ +1 & +1 & -1 & -1 & -1 & -1 & +1 & +1 \\ -1 & +1 & +1 & -1 & +1 & -1 & -1 & +1 \end{bmatrix} \quad (M2)$$

The matrix of results, shown in Table 4 can be written as matrix Y (M3):

$$Y = \begin{bmatrix} 25 \\ 42 \\ 76 \\ 45 \\ 81 \\ 5 \\ 66 \\ 15 \end{bmatrix} \quad (M3)$$

Multiplying the matrixes X^t and Y, as shown in Eq. 2, will be useful both for calculating the effects and the coefficients:

$$(X^t)Y = \begin{bmatrix} 355 \\ -141 \\ 49 \\ -21 \\ -23 \\ -113 \\ -59 \\ 73 \end{bmatrix} \tag{2}$$

The effects can be calculated by the Eq. 3:

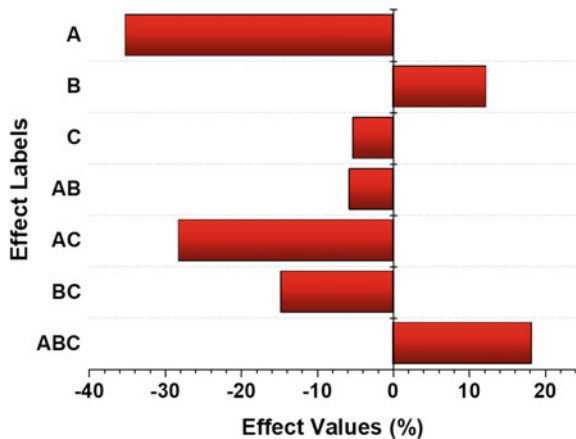
$$Effect(i) = \frac{(X^t)Y}{n/2} \tag{3}$$

The effects calculated are shown in Fig. 2.

From Fig. 2, one can notice that except for the effect of the of the factor B, and the tertiary interaction ABC, all other effects had negative values. For the primary effects A, B, and C a negative value means that moving from the lower to the upper level of these factors, leads to a decrease in the response variable, in this case, the yield. Similarly, a positive effect means that switching from the lower to upper level leads to an increase in the response variable.

For the secondary effects, such as AB, AC, and BC, an increase in the effect means that the response variable increases when the product between the levels of the two factors switch from negative to positive. The interpretation is similar to the tertiary effect, such as ABC.

Fig. 2 Graph showing the effect value for each one of the primary effects and interactions possible for the 2³ factorial design. The effects were calculated according to Eq. 3



2.5.1 The Empirical Model

As previously told, a 2^k factorial model can produce a polynomial equation where all the terms are linear; in general, the empirical model can be described by the Eq. 4:

$$y = b_0 + \sum_{i=1}^k b_i X_i + \sum_{1 \leq i < j}^k b_{ij} X_i X_j + \xi \tag{4}$$

where: b_0 the independent term related to the average of the response of all experiments, b_i or b_{ij} are the coefficients for each term, the X_i or X_j are the coded values of each factor, and ξ is the residual associated to the experiment.

For a factorial 2^k , the empirical model contains 2^k terms, being one term for each one of the effects plus the independent term. The residual term ξ is not explicitly written in the equation. In this sense, the empirical model equations for 2^2 , 2^3 , and 2^4 designs are shown, respectively, in the equations varying from 5 to 7:

$$y = b_0 + b_A X_A + b_B X_B + b_{AB} X_A X_B \tag{5}$$

$$y = b_0 + b_A X_A + b_B X_B + b_C X_C + b_{AB} X_A X_B + b_{AC} X_A X_C + b_{BC} X_B X_C + b_{ABC} X_A X_B X_C \tag{6}$$

$$y = b_0 + b_A X_A + b_B X_B + b_C X_C + b_D X_D + b_{AB} X_A X_B + b_{AC} X_A X_C + b_{AD} X_A X_D + b_{BC} X_B X_C + b_{BD} X_B X_D + b_{CD} X_C X_D + b_{ABC} X_A X_B X_C + b_{ABD} X_A X_B X_D + b_{ADC} X_A X_D X_C + b_{BDC} X_B X_D X_C + b_{ABCD} X_A X_B X_C X_D \tag{7}$$

Each one of the b_i or b_{ij} coefficients can be calculated by dividing the Eq. 2 by the number of experiments; in other words, the coefficients can be calculated according to Eq. 8:

$$b(i) = \frac{(X^t)Y}{n} \tag{8}$$

So, for the 2^3 factorial design, we are working on, the empirical model is shown in Eq. 9:

$$Yield(\%) = 44.4 - 17.6X_A + 6.1X_B - 2.6X_C - 2.9X_A X_B - 14.1X_A X_C - 7.4X_B X_C + 9.1X_A X_B X_C \tag{9}$$

2.5.2 Judging the Significance of the Effects to Refine the Empirical Model

Equation 9 presents all the eight possible terms for the empirical model. However, not all the terms will be significant. To judge which terms will be significant we have to decide which effects are significant using statistical tests. The coefficients related to the insignificant effects will be discarded from the model.

To have a rough estimate about which effects might be significant, the effects can be squared, and then, divided by the summation of all values, and multiplying by 100%, as shown in the Fig. 3.

Figure 3 shows that effects A, AC, and ABC are the three bigger ones. The summation of these three effects accounts for about 85% of all the effects. We can affirm, almost unequivocally, that these three effects are significant. Contrastingly, we can also claim that the effect C, which is smaller than 1%, is insignificant. But how about the other four effects? Are they significant or not?

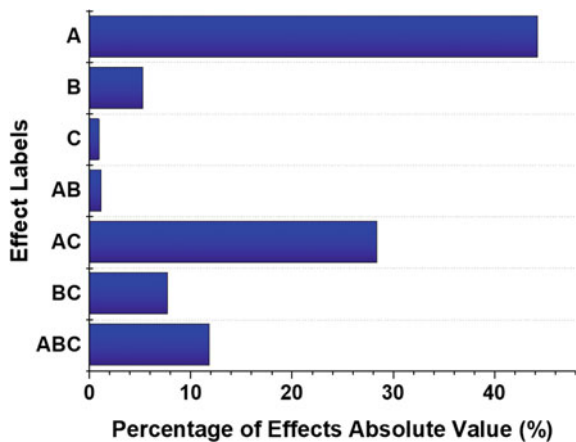
To answer this question, we need some statistical tests. One of the most popular tests is critical t-student, which is shown in Eq. 10:

$$critical - t = s_{Effect} \times t(DoF; p) \tag{10}$$

where s_{Effect} is defined as the standard deviation of the effects and $t(DoF; p)$ is the value obtained from a t-Student table with the number of degrees of freedom (DoF) from which s_{Effect} was calculated, and p is the probability. For instance, if the desired probability is 95%, the researcher should look for the t-student value with $p = 0.05$ in the t-Student table.

The s_{Effect} can in principle be simply calculated as the square root of the variance of the effects (s_{Effect}^2), from Eq. 11 [9]:

Fig. 3 Graph showing the percentage of effects absolute value for each one of the primary effects and interactions possible for the 2^3 factorial design



$$s_{Effect}^2 = \frac{4s_e^2}{\sum_{i=1}^n r_i} \quad (11)$$

where s_e^2 is an estimative of the variances, which can be calculated from Eq. 12, and r_i is the number of replicas. For instance, if each experiment was done twice, $r_i = 2$

$$s_e^2 = \frac{\sum_{i=1}^n [(r_i - 1)s^2]}{\sum_{i=1}^n [(r_i - 1)]} \quad (12)$$

In fact, in Eq. 12 the term $(r_i - 1)$ is particularly the degrees of freedom used in order to calculate the estimative of the variances, and s^2 is the variance for each experimental condition, as shown in Eq. 13:

$$s^2 = \frac{\sum_{i=1}^r (y_i - \bar{y})^2}{(r_i - 1)} \quad (13)$$

where y_i is each individual result of the replica, \bar{y} is the average of each individual result from the replicas, and r is the number of replicas.

After calculating critical-t using Eq. 10, the critical-t value is compared to the absolute value of each effect, and only the effects having absolute values higher than the critical-t will be considered significant, in that probability level p.

The best way to obtain all the variances necessary to calculate the critical-t is by performing all the experiments with replicas since it allows to calculate sequentially s^2 , s_e^2 , s_{Effect}^2 , from Eqs. 11, 12, and 13, respectively.

However, if no replicas were made for any of the experiments, it is still possible to obtain the variances necessary to calculate t-value. Yet, there are distinct ways to accomplish this task, a popular and prudent one is to perform additional experimental with all the factors fixed at the central point.

For quantitative factors, the central point is defined as the average between the lower and upper levels, and it has the coded value equal to zero. Table 8 is an adaptation of Table 2, including the central point for each factor.

As such, the experiment at the central point was then performed in triplicate, and the following results were obtained for the yield, as shown in Table 9.

Table 8 The factors with their respective limits and central points represented as coded (in parenthesis) and uncoded values

Factor	Lower limit	Central point	Upper limit
pH = A	8 (-1)	11 (0)	14 (+1)
Temperature (°C) = B	25 (-1)	55 (0)	85 (+1)
Catalyst concentration (mol L ⁻¹) = C	1 × 10 ⁻⁴ (-1)	3 × 10 ⁻⁴ (0)	5 × 10 ⁻⁴ (+1)

Table 9 Yield obtained for the experiments performed in the central point using triplicates

Factors			Yield (%)		
A	B	C	Exp 1	Exp 2	Exp 3
0	0	0	41	47	50

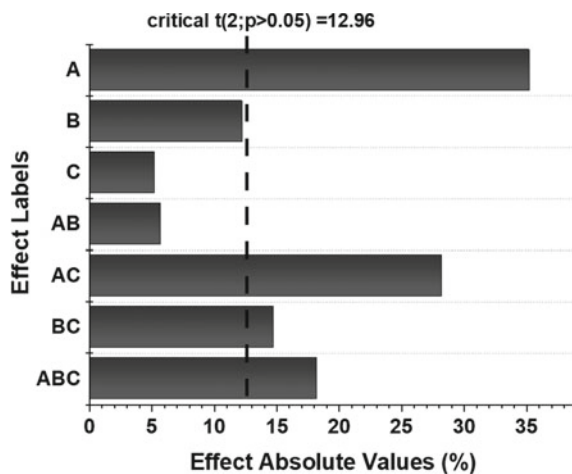
Table 10 Average yield, degrees of freedom, variances, standard deviation of the effect, tabled t-student value and, the critical-t value with 95% confidence obtained for the experiments performed in the central point using triplicates

Parameter	Value
Average yield	46
Degrees of freedom	2
Variance (s^2 and s_e^2)	14
S_{effect}^2	18.67
S_{effect}	4.32
t(2; 0.05)	2.92
Critical-t	12.6

The values for average, degrees of freedom, and variance (s^2 and s_e^2), S_{effect}^2 , S_{effect} , t-student (2; 0.05), and critical-t are shown in Table 10.

The graph shown in Fig. 4 is called Pareto chart, it is a bar graph where in the Y-axis all the effects are categorized, and in the X-axis the absolute value of the effects are presented. Then, a vertical line is fixed on the X-axis over the critical-t value. From the Pareto chart we can see that the effects higher than the critical-t are the pH (A), the secondary interaction between pH and catalyst concentration (AC), and between temperature and catalyst concentration (BC), and the tertiary interaction among the three factors (ABC). Notice that the Pareto chart confirmed the initial guess based on Fig. 3 that the effects A, AC, and ABC are significant. Also, the

Fig. 4 Pareto chart showing which effects are higher (if so, significant) than the critical-t



Pareto chart was essential to confirm that BC is significant, whereas the effect B is insignificant, although it is very close to the critical-t value.

Now that we decided which effects are significant, based on a statistical test. We can exclude from the model (Eq. 9) the coefficients related to the insignificant values. So, the model describing the factorial design is given by Eq. 14:

$$Yield(\%) = 44.4 - 17.6X_A - 14.1X_A X_C - 7.4X_B X_C + 9.1X_A X_B X_C \quad (14)$$

2.5.3 Assessing the Quality of the Model Using Analysis of Variance (ANOVA) Table

Replacing the coded values for X_A , X_B , and X_C on Eq. 14, it was possible to calculate the yield (%) predicted by the model for each one of the experiments performed, as shown in Table 11.

A standard method to assess the quality of the model by using three parameters called the sum of squares (SS), they are: the sum of square (SS) for the mean, for the regression, and for the residuals, and they are defined according to Eqs. 15–17:

$$SS_{mean} = \sum (y_i - \bar{y})^2 \quad (15)$$

$$SS_{regression} = \sum (\hat{y}_i - \bar{y})^2 \quad (16)$$

$$SS_{residual} = \sum (y_i - \hat{y}_i)^2 \quad (17)$$

Table 11 Comparison between the yield (%) obtained experimentally and predicted by the model represented by Eq. 14

A	B	C	Experimental	Predicted
-1	-1	-1	25	31.4
1	-1	-1	42	42.6
-1	1	-1	76	64.4
1	1	-1	45	39.2
-1	-1	1	81	92.6
1	-1	1	5	11
-1	1	1	66	59.6
1	1	1	15	14.4

Table 12 Analysis of variance (ANOVA) Table for the 2^3 factorial design

ANOVA table			
Source of variation	Sum of square	Degrees of freedom	Mean squares
Mean	5603.88	7	800.55
Regression	5169.12	4	1292.28
Residual	421.40	3	140.47
R^2 ($SS_{\text{regression}}/SS_{\text{mean}}$)	0.9224		
$MS_{\text{regression}}/MS_{\text{residual}}$	9.20		
F-test for 4/3 degrees of freedom with 95%	5.39		

where: y_i is the value obtained experimentally, \hat{y}_i being value predicted according to the model, and the \bar{y} is the average of all experimental values.

Note that each sum of squares has a certain number of degrees of freedom which can be associated with them. It is known that for SS_{residual} the number of degrees of freedom is found to be equal to the difference of the number of independent experiments (8, in this example) and the number of parameters contained in the equation describing the model (5, in this example), so SS_{residual} has 3 degrees of freedom. For the $SS_{\text{regression}}$ the number of degrees of freedom is equal to the number of parameters (5, in this example) minus 1, so the $SS_{\text{regression}}$ has 4 degrees of freedom. Finally, the number of degrees of freedom of SS_{mean} is equal to the number of degrees of freedom for SS_{residual} plus $SS_{\text{regression}}$, so 7 degrees of freedom.

Hence, the mean square (MS) for regression, residual, and mean was then calculated by dividing each sum of squares by its respective number of degrees of freedom. So, Table 12 presents the complete ANOVA table for the example analyzed.

There are two criteria used to assess the model quality through the ANOVA table. The first one is based on the coefficient of determination (R^2), which is the ratio between the $SS_{\text{regression}}$ and SS_{mean} . An R^2 as close as to 1 represents a better quality of the model. In this example, an R^2 equal to 0.9224 means that 92.24% of the variation is explained by the model, whereas only 7.76% is explained by the residuals.

The second parameter is the ratio between $MS_{\text{regression}}$ and MS_{residual} . This value is in general compared to the F-test value with 95% of confidence, and the number of degrees of freedom in the numerator as the same number of degrees of freedom as $MS_{\text{regression}}$. And the number of degrees of freedom in the denominator as the same number of degrees of freedom as MS_{residual} . As the ratio $MS_{\text{regression}}/MS_{\text{residual}}$ (9.20) is higher than the F-test with 95% confidence, and 4/3 degrees of freedom (5.39), we can conclude that the model is appropriately fitted to the data.

For most of the researchers, the model described by Eq. 14 would have enough quality, which eliminates the need to perform additional experiments for optimization to obtain a model with quadratic terms, as the ones to be discussed in Sect. 2.6.

2.6 Optimization Steps

Depending on the situation studied, an empirical model where all the terms in the polynomial are linear may not be satisfying. In this sense, the researcher will have to use experimental designs able to produce polynomials containing quadratic terms, such as the one generically represented by Eq. 18:

$$y = b_0 + \sum_{i=1}^k b_i X_i + \sum_{i=1}^k b_{ii} X_i^2 + \sum_{1 \leq i < j}^k b_{ij} X_i X_j + \xi \tag{18}$$

Compare Eq. 18 with Eq. 4, and notice that there are no quadratic terms in the Eq. 4.

In this section, we will be introduced to the basics of four designs able to produce polynomial models containing quadratic terms. The four designs to be studied are 3^k Factorial Design, Central Composite Design (CCD), Box-Behnken Design, and Doehlert Design. In all these designs, all the factors are studied in more than two levels.

The group formed by these designs is called Response Surface Methodology (RSM), as the equations described by each model can be converted in a tri-dimensional graph called response surface. In none of these models there will be a detailed example, like the one we presented for 2^k factorial design. Readers interested to have a more in-depth knowledge about any one of these designs are encouraged read the references cited in this section or the ones in Sects. 3 and 4.

Also, specifically about RSM, the books: *A Comprehensive Guide to Factorial Two-level Experimentation* by Mee [6], and *Design and Analysis of Experiments* by Dean et al. [10] are good resources for readers avid for learning more about each one of the RSMs.

2.6.1 Three Level Factorial Design (3^k Design)

In the 3^k factorial design, all the factors have three levels $(-1, 0, +1)$. Although the 3^k design implementation is not so complicated due to its similarity to 2^k designs, it requires a relatively large number of experiments. For this reason, the 3^k design is used to study a few factors, generally, two or three [11].

2.6.2 Central Composite Design (CCD)

The Central Composite Design (CCD) is made up by the combination of the following features [3, 9]:

- (i) A full 2^k factorial design or a fractional factorial design 2^{k-p} .

Table 13 Matrix of experiments for a 2^2 CCD factorial design

2 ² factorial design		
X _A	X _B	2 ² factorial design
-1	-1	
+1	-1	
-1	+1	
+1	+1	
0	0	Central point experiment
-α	0	Axial point experiments
+α	0	
0	-α	
0	+α	

Table 14 Matrix of experiments for a 2^3 CCD factorial design

2 ³ factorial design			
X _A	X _B	X _C	2 ³ factorial design
-1	-1	-1	
+1	-1	-1	
-1	+1	-1	
+1	+1	-1	
-1	-1	+1	
+1	-1	+1	
-1	+1	+1	
+1	+1	+1	
0	0	0	Central point experiment
-α	0	0	Axial point experiments
+α	0	0	
0	-α	0	
0	+α	0	
0	0	-α	
0	0	+α	

- (ii) Central point experiments, where all the factors have coded values equal to zero.
- (iii) Experiments in the axial points. In these experiments, one factor will have coded value equal to $\pm\alpha$. These $\pm\alpha$ values are located in the axes of the coordinated system, and in distance $\pm\alpha$ from the origin of the system.

Tables 13 and 14 show the matrix of experiments for a CCD design having a 2^2 and 2^3 factorial as screening designs [3].

From the matrix of experiments, one can conclude that the total number of experiments for a CCD, disregarding any replicas, is equal to the Eq. 19:

Table 15 Number of experiments at axial level, axial levels, and total number of experiments for CCD factorial designs according to the number of factors

Number of factors (k)	2	3	4	5	5	6	6
p in 2^{k-p}	0	0	0	0	1	0	1
Number of Experiments in axial levels ($\pm\alpha$)	4	6	8	10	10	12	12
$+\alpha$ values	1.414	1.682	2.000	2.378	2.000	2.828	2.378
Total number of experiments	9	15	25	43	27	77	45

$$\text{NumberofExperiments} = 2^k + \text{CentralPoint} + 2k \tag{19}$$

where the 2^k is the number of experiments related to the 2^k factorial, the Central Point is the experiment carried out in the central point, and $2k$ is the number of the experiments related to the axial points $\pm\alpha$.

The coded values $\pm\alpha$ can be figured out according to Eq. 20 [9].

$$\alpha = \sqrt[4]{2^k} \tag{20}$$

In the CCD, any coded value can be decoded according to Eq. 21. This equation is also valid to convert the $\pm\alpha$ to their respective decoded values [9]:

$$x_i = \frac{z_i - \bar{z}}{\Delta z / 2} \tag{21}$$

where x_i is the coded value for the factor i , z_i is the decoded value for the factor i , \bar{z} is the decoded value for the central point for the factor i , and the Δz is the difference between the upper (+) and lower (-) levels for the factor i .

Table 15 summarizes how many experiments should be made in the axial levels $\pm\alpha$, the value of α , and the total number of experiments according to the k value in 2^{k-p} .

2.6.3 Box-Behken Designs

Similarly to the three levels factorial design the Box-Behken Desing (BBD) is a three levels (-1, 0, +1) for all factors. The number of experiments to be performed, disregarding replicas, according to the number of factors (k) is given by the Eq. 22 [12]:

$$\text{NumberofExperiments} = 2k(k - 1) + \text{CentralPoint} \tag{22}$$

The conversion between the coded and uncoded values in a BBD is given by Eq. 23 [13]:

$$x_i = \left(\frac{z_i - \bar{z}}{\Delta z} \right) \quad (23)$$

where x_i is the coded value for the factor i , z_i is the decoded value for the factor i , \bar{z} is the decoded value for the central point for the factor i , and the Δz is the difference between the upper (+) and lower (-) levels for the factor i .

One advantage of the BBD is that there is no experiment where the factors are taken all of them at the same time in the lower limit nor the upper limit. This fact avoids that experiments are carried out at extreme conditions and may avoid unsatisfactory or abnormal results to happen [14].

For more details about BDD matrix, readers are encouraged to read the review paper by Ferreira et al. [14].

2.6.4 Doehlert Designs

A feature differing Doehlert Designs (DD) from CCD and BBD is that DD does not have the same number of levels for all the factors. For instance, in a DD with $k = 2$, one factor has three levels (with coded values equal to -8.666 , 0 , $+8.666$), and the other has five levels (with coded values equal to -1 , -0.5 , 0 , $+0.5$, $+1$). For a DD with $k = 3$, one factor has five levels (with coded values equal to -1 , -0.5 , 0 , $+0.5$, $+1$), the second one has seven levels (with coded values equal to -0.866 , -0.577 , -0.289 , 0 , $+0.289$, $+0.577$, $+0.866$), and the third factor has three levels (with coded values equal to -0.866 , 0 , $+0.866$) [11, 12]. In this sense, we can conclude that DD requires the following number of experiments, disregarding replicas, according to k value as shown in Eq. 24:

$$\text{NumberofExperiments} = k^2 + k + \text{CentralPoint} \quad (24)$$

The conversion between the coded and uncoded values in a DD is given by Eq. 25 [12]:

$$x_i = \left(\frac{z_i - \bar{z}}{\Delta z} \right) \alpha \quad (25)$$

where x_i is the coded value for the factor i , z_i is the decoded value for the factor i , \bar{z} is the decoded value for the central point for the factor i , the Δz is the difference

between the upper (+) and lower (−) levels for the factor i , and α is the coded value limit for the factor i .

For verifying examples about DD matrix, readers are encouraged to read the review paper by Ferreira et al. [12].

2.6.5 Comparison Between the Different Response Surface Methodologies

To compare the four RSMs presented in this section, we take advantage of the efficiency parameter, which is defined by the ratio between the number of coefficients present in the model of the RSM and the number of experiments necessary to accomplish that RSM [8]. Table 16 presents the number of coefficients, the number of experiments, the efficiency, according to the number of factors for the four RSMs presented.

From Table 16, regardless of the number of factors, the DD presents a lower number of experiments and higher efficiency. Also notice that the 3^k design is not practical for $n \geq 4$ [15].

3 Factorial Design of Experiments Applied to Nanomaterials Production and Performance

Nanomaterials are recognized for presenting outstanding properties when compared with their bulk-like versions. In this sense, it is necessary to develop synthetic methods able to precisely tune properties such as nanoparticle size, surface area, bandgap, and photoluminescent emission. To be able to obtain a fine control over these properties, usually, many factors need to be considered. Most of the time, a comprehensive study would require a massive number of experiments. For making the production process more efficient, the factorial design can be used to sort the significant factors. Then, it can be used to derive models for predicting how much that response property could be in a previously untested condition. In this section, we will see five examples where the factorial design was applied to obtain as the response variables different properties of nanomaterials.

3.1 Optimization of Copper (Cu) Nanoparticle Size Using 2^2 Factorial Design

The first paper of this section deals with the synthesis of copper (Cu) nanoparticles. Granata and co-workers studied how different capping agents, such as cetyl trimethyl

Table 16 Comparison among the four RSMs presented regarding the number of experiments and efficiency

Number of factors	Number of coefficients		Number of experiments				Efficiency			
	6	3 ^k	CCD	BBD	DD	3 ^k	CCD	BBD	DD	DD
2	6	9	9	N/A	7	0.67	0.67	N/A	0.86	0.86
3	10	27	15	13	13	0.37	0.67	0.77	0.77	0.77
4	15	81	25	25	21	0.19	0.60	0.60	0.71	0.71
5	21	243	43	41	31	0.09	0.49	0.51	0.68	0.68
6	28	729	77	61	43	0.04	0.36	0.46	0.65	0.65

ammonium bromide (CTAB), sodium dodecyl sulfate (SDS), and polyvinylpyrrolidone (PVP). And also, how different reducing agents, such as hydrazine and glucose, can influence the mean particle size and the stability against oxidation of the Cu nanoparticles [16].

By combining the three available capping agents with the two available reducing agents, the authors designed six different 2^2 factorial designs. The response variables analyzed were the mean and standard deviation of the particle size of the Cu nanoparticles as estimated by histograms counting 500 particles from scanning electron microscopy images. The authors were aiming to minimize the mean particle size and standard deviation since smaller Cu particles are more likely to present the surface plasmon resonance (SPR) phenomenon.

For all the designs, the temperature and initial pH were fixed at 85 °C and pH equal to 10. The levels for the surfactant and reducing agent factor for each one of the six 2^2 factorial designs are shown in Table 17 [16].

When glucose is used as the reducing agent, for design 1, only the glucose had a significant effect, and this effect was around +11.6 nm. As this effect is positive, it means that increasing glucose concentration from 0.2 to 0.5 mol L⁻¹ led to an increase of 11.6 nm in the size of Cu nanocrystals. For design 2, both the capping agent and reducing agent had significant effects. The glucose had a negative effect, whereas the CTAB had a positive effect. These results mean that the Cu mean particle

Table 17 The six 2^2 factorial designs used to analyze the interactions between capping and reducing agents—data by Granata et al. [16]

Factor	Lower limit (mol L ⁻¹)	Upper limit (mol L ⁻¹)
<i>Factorial design 1</i>		
Capping agent	SDS 0.1	SDS 0.2 mol L ⁻¹
Reducing agent	Glucose 0.2	Glucose 0.5
<i>Factorial design 2</i>		
Capping agent	CTAB 0.1	CTAB 0.2
Reducing agent	Glucose 0.2	Glucose 0.5
<i>Factorial design 3</i>		
Capping agent	PVP 0.1	PVP 0.2
Reducing agent	Glucose 0.2	Glucose 0.5
<i>Factorial design 4</i>		
Capping agent	SDS 0.1	SDS 0.2
Reducing agent	Hydrazine 0.2	Hydrazine 0.5
<i>Factorial design 5</i>		
Capping agent	CTAB 0.1	CTAB 0.2
Reducing agent	Hydrazine 0.2	Hydrazine 0.5
<i>Factorial design 6</i>		
Capping agent	PVP 0.1	PVP 0.2
Reducing agent	Hydrazine 0.2	Hydrazine 0.5

size increased when the glucose concentration decreased or CTAB concentration increased. Finally, for design 3, not only glucose and PVP presented significant effect, but, the interaction between these two factors was significant as well. For all cases, the effects presented were negative, which means that by increasing the level of all variables from lower to the upper limit led to a decrease in the Cu mean particle size.

When hydrazine is used as the reducing agent, for design 4, only hydrazine and SDS had significant effects, being the hydrazine positive and the SDS negative. So, the Cu particle size increased with increasing hydrazine concentration a decreasing the SDS concentration. For design 5, both hydrazine and CTAB had significant effects, both of them positive. These results mean that the Cu mean particle size increased when the hydrazine or CTAB concentrations increased. Finally, for design 6, hydrazine and PVP presented a significant effect, following the same trend observed in design 4. Interestingly, for none of the designs, the interaction between capping and reducing agents showed significant effects.

After calculating the significant effects for each factorial design, the authors did not advance on using the factorial design to estimate a model for the mean particle size or standard deviation for the nanoparticles. From effects estimation the authors concluded that the PVP was probably the best capping agent for their purpose, as it is the capping agent that, for either reducing agents, had the highest effect on changing the nanoparticle size.

To subdivide all the data in six smaller 2^2 factorial designs was a wise decision, and it simplified a lot of the data analysis. Although this simplification eliminated, to some extent, the holistic character of the factorial design. To obtain a more comprehensive model would require that each factor to have a different number of levels.

3.2 Optimization of Silica Microspheres Size Using a 2^3 Factorial Design a Linear Response Surface Model

Silica (SiO_2) microspheres are multifunctional materials, having applications in colloidal templating, photonic crystals, polymer encapsulation, to cite a few of them [17]. SiO_2 microspheres are prepared through the alkaline hydrolysis of silicon alkoxides in a water–ethanol solvent mixture. A common source of silicon is the tetraethyl orthosilicate (TEOS), whereas the reaction is usually catalyzed by water. The diameter of microspheres depends on an accurate control of the quantities of the reactants, catalysts, and solvents, for instance, TEOS, NH_3 , and water. Considering that the diameter of the microspheres can determine its possible applications, to be able to control this feature systematically in a predictable way is a characteristic necessary for the synthetic method [18].

Aiming to obtain precise control over the diameter of SiO_2 microspheres, Arantes et al. used a 2^3 factorial design to study the effect of the factors number of moles

Table 18 The three factors and their levels in the 2^3 factorial designs used to control the size of SiO_2 microspheres—data by Arantes et al. [19]

Factor	Lower level	Upper level
NH_3 (mol)	3.0×10^{-2}	6.0×10^{-2}
TEOS (mol)	2.0×10^{-2}	4.0×10^{-2}
H_2O (mol)	0	1.0×10^{-1}

of ammonia, tetraethyl orthosilicate (TEOS), and water in the particle size of SiO_2 microspheres [19]. As such, the levels of each factor are shown in Table 18.

Only NH_3 and H_2O presented significant primary effects. The other significant effect was the interaction between TEOS and H_2O . After having concluded the significant effects, the authors calculated the coefficients related to each one of them and obtained a linear polynomial model to predict the SiO_2 particle size out of the initially performed experimental conditions, as shown in Eq. 26:

$$Y = 158.82 + 97.52X_1 + 47.97X_3 + 29.092X_2X_3 \quad (26)$$

where X_1 is the coded values for the number of moles of NH_3 , X_2 is the number of moles of TEOS, and X_3 is the number of moles of water.

This model equation allowed the authors to plot a response surface graph by fixing NH_3 either in its lower (0.3 mol) or higher (0.6 mol) levels and varying the other two factors, as shown in Fig. 5.

From Fig. 5, we notice that both graphs presented a similar behavior. In other words, by increasing the amount of H_2O and TEOS led to a maximization of the particle size of the SiO_2 microspheres. However, when NH_3 is fixed on its upper level, the SiO_2 particle size predicted is much higher than ones predicted by fixing NH_3 on its lower level and varying H_2O and TEOS.

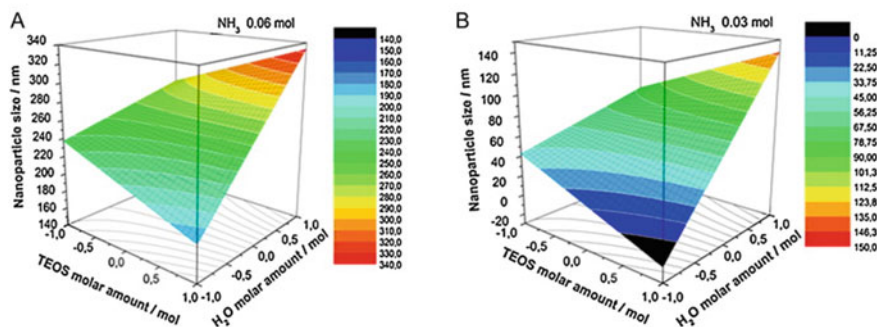


Fig. 5 Surface responses **a** by fixing the NH_3 molar amount in the level +1 (0.06 mol) and **b** by fixing the NH_3 molar amount in the level -1 (0.03 mol). Adapted from reference number [19], with permission from Elsevier

To confirm the quality of the model, the authors calculated the analysis of variance (ANOVA) table, and it revealed a coefficient of determination (R^2) equal to 95%, which means that 95% of the variation observed can in principle be explained by the obtained model. Finally, to experimentally confirm the applicability of the model, the authors performed an experiment where the coded values for NH_3 , TEOS, and H_2O were, respectively, equal to -1, 0, and 0.5. By plugging these values into Eq. 26, it was predicted that the particle size should be around 85 nm. And in practice, the result of the experiment performed revealed that the SiO_2 particle size was very close 85 nm. This result showed a nice agreement in relation to the experimental data and the values predicted by the model.

3.3 Optimization of Manganese Sulfide (MnS) Thin-Films Thickness Using a 2^4 Factorial Design and Dohelert Approach for Quadratic Response Surface

To be able to control thin film thickness is an essential property of a proper deposition procedure. In this sense, Hannachi and co-workers used a 2^4 factorial to study the effects of time, temperature, initial concentrations of manganese acetate and thioacetamide on the thickness of manganese sulfide (MnS) deposited via chemical bath deposition onto glass substrates [20].

The levels were studied for each one of the factors, as shown in Table 19.

The authors found that the deposition time, temperature, and manganese acetate initial concentration had significant primary effects. All these three factors had positive effects, which means that increasing either one of them from their lower to the upper levels would lead to an increase in the film thickness. On the other hand, the thioacetamide concentration effect was not significant. The secondary interactions involving the deposition time, temperature, and manganese acetate initial concentration when taken at two by two at a time also were significant. Endly, the tertiary interaction combining the three significant factors was significant as well. After judging the significance of the effects, the authors obtained the eight terms linear-polynomial model describing the thin-film thickness:

$$Y = 483 + 204.3X_1 + 159.5X_2 + 189.4X_3 + 98.3X_1X_2 + 106.6X_1X_3 + 159.1X_2X_3 + 71.4X_1X_2X_3 \quad (27)$$

Table 19 The four factors and their levels in the 2^4 factorial designs used to control the MnS thin-film thickness—data by Hannachi et al. [20]

Factor	Lower level	Upper level
Time (h)	1	24
Temperature ($^{\circ}\text{C}$)	Room temp	70
Mn acetate conc. (mol L^{-1})	0.5	2
Thioacetamide (mol L^{-1})	0.5	2

where X_1 is the coded values for the deposition time, X_2 is deposition temperature, and X_3 is the concentration of manganese acetate.

The conclusions obtained in the 2^4 factorial design served as the foundation to further optimize the model using a Doehlert approach, studying only the three factors that were significant in the 2^4 screening factorial design. This Doehlert design allowed the authors to obtain a quadratic model (Eq. 28), and a set of response surface graphs.

$$Y = 349.0 + 136.5X_2 + 119.2X_3 - 129.0X_1^2 - 187.0X_2^2 - 124.0X_3^2 + 98.2X_1X_2 + 148.5X_2X_3 \tag{28}$$

where X_1 is the coded values for the deposition time, X_2 is deposition temperature, and X_3 is the concentration of manganese acetate.

The first response surface graph was plot fixing the thioacetamide concentration at 0.5 mol L^{-1} and varying the deposition temperature and time. The second response surface graph was plot fixing the thioacetamide concentration at 0.5 mol L^{-1} and varying the manganese acetate initial concentration and deposition time. Finally, the third surface was plot fixing the thioacetamide concentration at 0.5 mol L^{-1} and varying the manganese acetate initial concentration and deposition temperature. The three response surfaces are shown in Fig. 6.

By analyzing the three response surface plots, it was concluded that the MnS thin-film thickness was maximized (thickness around 330–400 nm), when the deposition temperature was $60 \text{ }^\circ\text{C}$, time was 20 h, manganese acetate concentration around 1.6 mol L^{-1} , and thioacetamide concentration equal to 0.5 mol L^{-1} .

To be able to indicate a narrow range of conditions that would lead to maximization of the thin-film thickness demonstrates how resourceful factorial design and response surface methodologies are. This affirmation comes from the fact that none of the conditions indicated as optimum were the same as the ones the authors initially used as levels in the 2^4 factorial.

The authors deposited a thin-film under the conditions deemed to produce the highest thickness. The structural characterization techniques indicated the MnS was

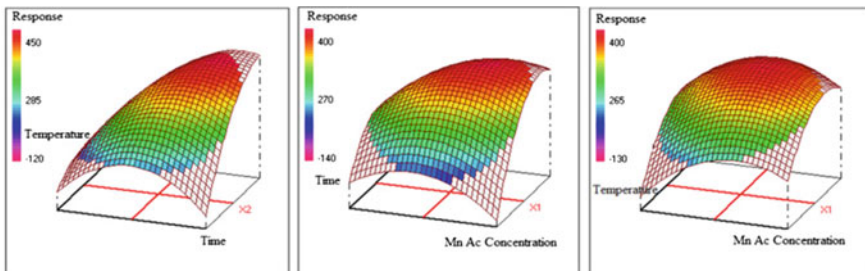


Fig. 6 Surface responses (left) varying time and temperature (middle) varying time and Mn acetate conc. (right) varying temperature and Mn acetate conc. Adapted from reference number [20], with permission from Elsevier

satisfactorily deposited onto the glass substrate. However, the authors failed to inform the thin-film thickness, which makes the readers unable to infer if the model used to produce the response surface graphs has a good agreement to the experimental data or not.

3.4 Optimization of Cellulose and Sugarcane Bagasse Oxidation Using a 2³ Factorial Design with Full Central Composite Design (FCCD)

The use of functional materials derived from natural sources or obtained from wastes is a procedure aligned with the Green Chemistry Principles, as long as the obtaining of these materials does not cause any environmental harm [21]. In this sense, Martins et al. studied the oxidation of cellulose and sugarcane bagasse by a simple procedure [22]. The oxidation procedure is based on stirring either the cellulose (Cel) or the sugarcane bagasse (SB) with phosphoric acid (H_3PO_4) and sodium nitrite (NaNO_2) for different time intervals.

To accomplish this goal, initially, the authors designed a 2³ factorial design, where the factors studied were the duration of the oxidation procedure (in hours), the volume of H_3PO_4 (in mL), and the mass of NaNO_2 (in g). The response variable was the number of carboxyl groups per gram of material, represented by the symbol n_{COOH} (in mmol/g), which can be taken as an indication of the successful oxidation of the initial material.

The Pareto plot revealed that for Cel, all the primary effects were significant, with the secondary effect between the volume of H_3PO_4 and the mass of NaNO_2 also being significant. For the SB, the Pareto plot revealed that only the primary effect related to the mass of NaNO_2 was significant. Additionally, the secondary effect between the volume of H_3PO_4 and the mass of NaNO_2 also was significant (Fig. 7).

Having concluded the significant factors for the oxidation of each one of the materials studied, the authors started to optimize the model by doing a full central composite design. This design was accomplished by a full central composite design (FCCD). For each one of the materials studied, this FCCD was carried out by performing the eight experiments predicted by the 2³ design, without replicas. Plus, the experiment in the central point, in triplicates, and six more experiments. Where, each one of these six, one of the factors assumed a + α or - α , whereas the two other factors were kept in the central point.

From the FCCD, the authors could obtain empirical models containing quadratic terms. These empirical models were used to plot the response surface graphs by fixing the reaction duration in 5 h, and varying the H_3PO_4 volume and NaNO_2 mass, as shown in Fig. 8.

The response surface graphs showed that, when the reaction duration is equal to 5 h, the n_{COOH} is maximized for H_3PO_4 volume between 11 and 19 mL, and NaNO_2

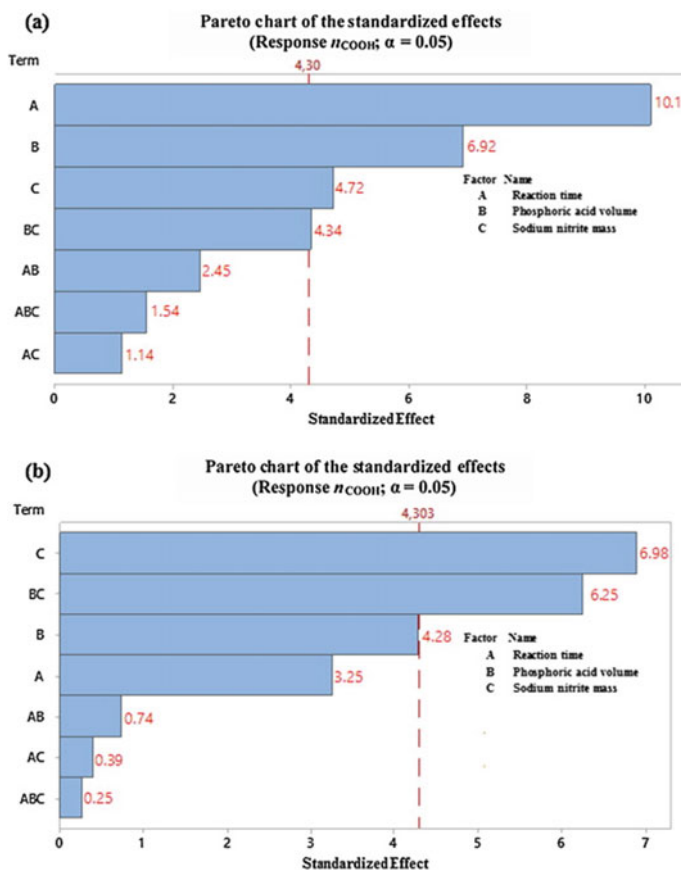


Fig. 7 Pareto charts for Cel (top) and SB (bottom). Adapted from reference number [22], with permission from Elsevier

volume between 500 and 970 mg. This conclusion agrees with the results initially obtained during the performance of the central point experiments.

After completing the full factorial design regarding the n_{COOH} , the authors used the products of Cel and SB oxidation to remove the dyes auramine O and crystal violet from simulated wastewater by adsorption. In general, the oxidated Cel presented better performance than the oxidated SB, for the removal of either of the dyes.

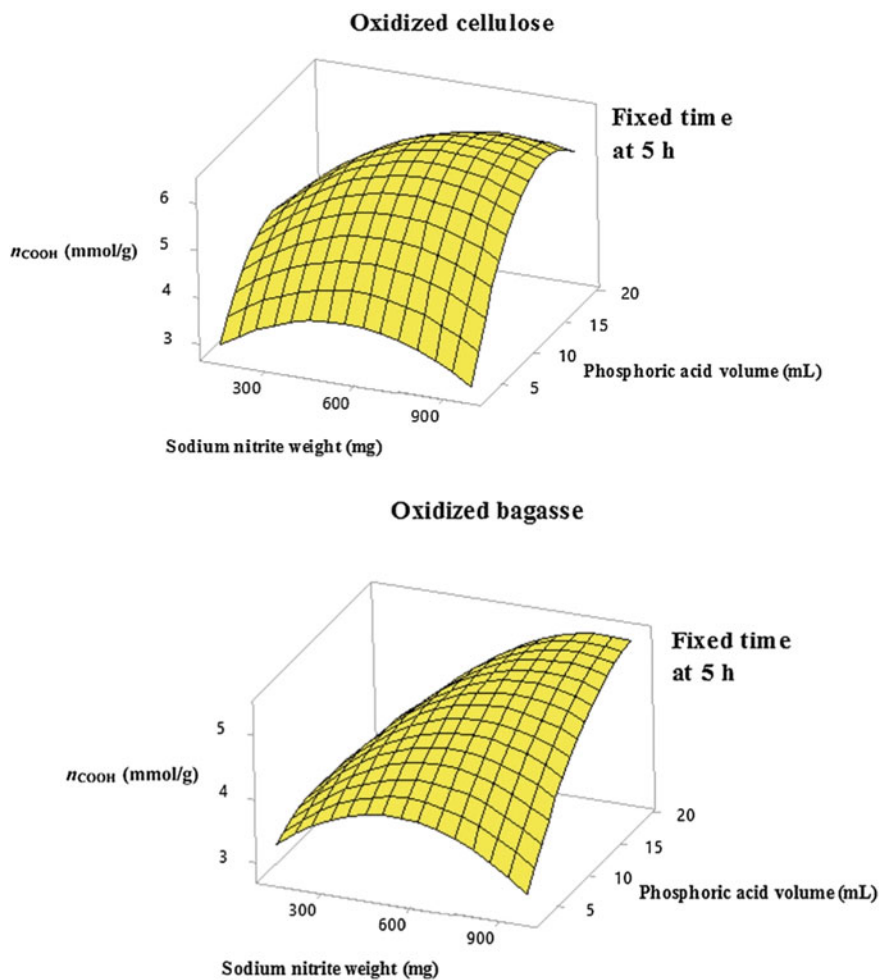


Fig. 8 Response surface graphs for Cel (top) and SB (bottom), by varying H_3PO_4 volume and NaNO_2 weight, the reaction duration was fixed at 5 h. Adapted from reference number [22], with permission from Elsevier

3.5 2^{5-1} Fractional Factorial Design with Box-Behnken Optimization—Improving Reproducibility Between Batches of Silver Nanoparticles Using an Experimental Design Approach

Silver nanoparticles (Ag NPs) are very versatile materials since they can be applied in many different fields, such as catalysis, biological sensors, antimicrobial activities,

DNA sequencing, surface-enhanced Raman spectroscopy, and information storage [23].

Ag NPs can be produced by the reduction of Ag^+ with gallic acid (GA, $\text{C}_7\text{H}_6\text{O}_5$) in alkaline pH, by stirring the reaction mixture in the dark, at room temperature. However, this procedure lacks reproducibility since the Ag NPs tend to have different size distributions according to the reaction batch [24]. With the goal to decrease this lack of reproducibility, Núñez et al. performed a two-level factorial design to study the effects of NaOH, AgNO_3 , and GA molar concentrations, also the effects of the reaction time and stirring speed [24]. So, the study had a total of five factors, with two-levels each. The response variable studied was a parameter called ψ , which was defined according to Eq. 29:

$$\psi = \frac{A_{\max}}{\lambda_{\max} \times FWHM} \quad (29)$$

In Eq. 29, A_{\max} is the absorption intensity of the band corresponding to the surface plasmon resonance (SPR), λ_{\max} is the wavelength of SPR band, and FWHM is the full-width at half-maximum of SPR band. The best ψ values are obtained when A_{\max} is maximized, and λ_{\max} and FWHM are both minimized, in other words, the ψ is better as it gets higher. And higher ψ means that Ag NPs were smaller and with a narrower size distribution [25].

As five factors were studied, a full two-level factorial design would lead to the performance of 32 experiments. To minimize the number of experiments to be done, the authors opted to do a fractional factorial design (FFD). In general, an FFD is symbolized as $2^{(k-p)}$. Where k is the number of factors, and p is the number of design generators. More specifically, in this paper, the authors carried out a 2^{5-1} factorial design. The number 5 represents the five factors ($[\text{NaOH}] = \text{A}$, $[\text{AgNO}_3] = \text{B}$, $[\text{GA}] = \text{C}$, time = D, and speed = E), and 1 represents the generator I = ABCDE.

The FFD was made up of sixteen experiments plus five experiments with all the factors in the central point. All experiments were performed with replicas. The lower and upper levels of each variable were defined, as shown in Table 20.

The Pareto chart indicated that the significant primary effects were the [GA], the reaction time, and $[\text{AgNO}_3]$. As shown in Fig. 9.

Table 20 The five factors and their levels in the 2^{5-1} factorial designs used to control the ψ in Ag NPs preparation—data by Núñez et al. [24]

Factor	Lower level	Central point	Upper level
[NaOH] ($\mu\text{mol L}^{-1}$)	500	750	1000
$[\text{AgNO}_3]$ ($\mu\text{mol L}^{-1}$)	50	75	100
[GA] ($\mu\text{mol L}^{-1}$)	5	12.5	20
Time (min)	10	30	50
Stirring speed	1	5.5	10

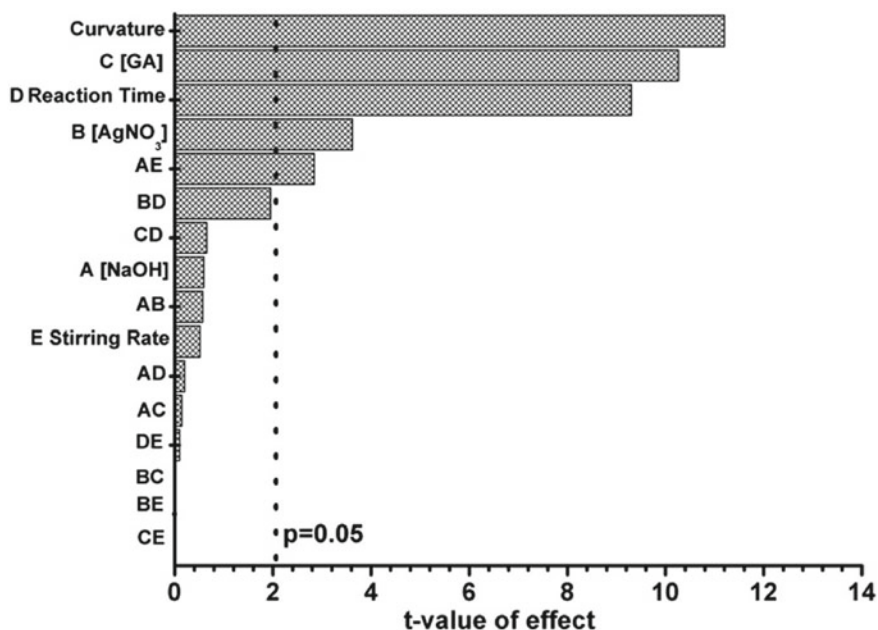


Fig. 9 Pareto chart showing the effects of ψ in Ag NPs synthesis. Adapted from reference number [24], with permission from Elsevier

After concluding the significant effects, the factorial designed continued by performing an optimization using the Box-Behnken design (BBD). The BBD is an incomplete three-level design to obtain a quadratic polynomial model. According to the number of experiments conducted is equal to $2k(k-1) + C_0$. Where k is the number of factors, in this case, $k = 3$, and C_0 is the number of experiments in the central point, in this case, $C_0 = 5$. In summary, 17 experiments were performed on this BBD. For the BBD, instead of using ψ as the response variable, the authors used A_{\max} , λ_{\max} , and FWHM separately.

For each one of the response variables (A_{\max} , λ_{\max} , and FWHM), quadratic polynomial equations were obtained, and response surface graphs were plotted by fixing either one of the factors ($[\text{AgNO}_3]$, $[\text{GA}]$ and reaction time). For the A_{\max} , it is maximized as $[\text{AgNO}_3]$, $[\text{GA}]$, and reaction time increase. The λ_{\max} is minimized when $[\text{AgNO}_3]$ increases, and $[\text{GA}]$ decreases. And the FWHM became narrower when $[\text{AgNO}_3]$ increased, and $[\text{GA}]$ decreased. The response surface graphs are shown for the λ_{\max} in Fig. 10.

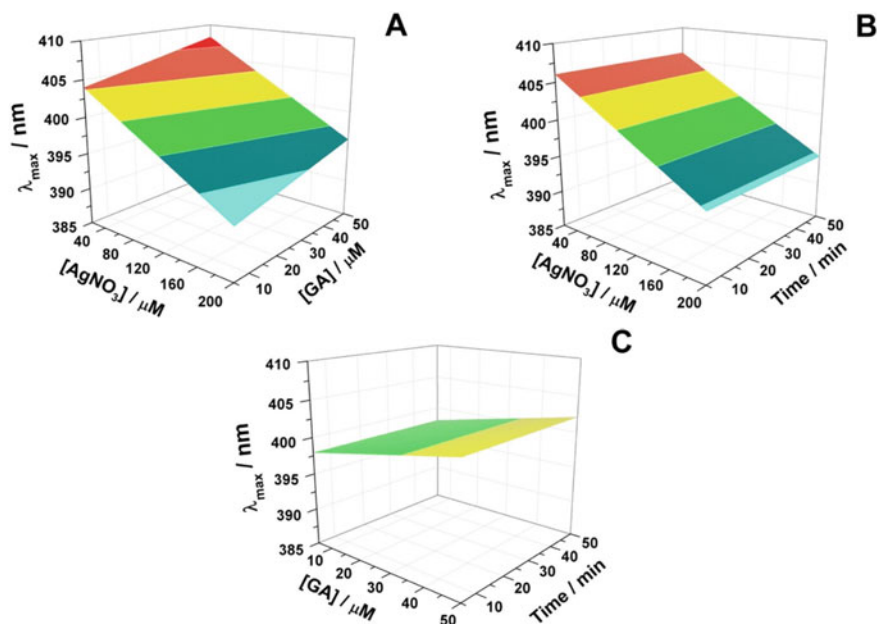


Fig. 10 Response surface graphs of λ_{\max} by varying **a** $[\text{AgNO}_3]$ and $[\text{GA}]$, **b** $[\text{AgNO}_3]$ and time, **c** $[\text{GA}]$ and time. Adapted from reference number [24], with permission from Elsevier

4 Factorial Design of Experiments Applied to Nanomaterials Production and Performance

The fields of Materials Science, Materials Chemistry, and Nanotechnology are all very broad. That being said, it would be impossible to cover every single possible application in a book chapter. In this sense, this part is intended to present some references related to four areas of application in Materials Science and Nanotechnology. They are nanoparticles preparation and characterization, drug encapsulation and delivery, wastewater remediation, and solar cell development.

For each one of these areas, around ten to twenty references, are presented classified according to the Factorial Design and Response Surface Methodology used on each paper, and the goal set by the papers. Unlike Sect. 3, there will not be any further detail about any paper. Instead, the readers are encouraged to read the tables and figure out if they get interested in the statistical methods or the theme of the paper. Then, they should feel free to consult these references independently. In order to show the relevance and the insertion of the factorial design of experiments in the current scientific literature, all examples presented were published between 2015 and 2020.

4.1 Design of Experiments Applied to Materials Synthesis and Characterization

See Table 21.

4.2 Design of Experiments Applied to Drug Encapsulation and Delivery

See Table 22.

4.3 Wastewater Remediation

See Table 23.

4.4 Design of Experiments Applied to Solar Cells Design and Performance

See Table 24.

5 Concluding Remarks

This chapter presented the theoretical bases of the factorial design and applications of the design of experiments in different areas of Materials Science and Nanotechnology. The depth and extent of the technique open up the possibility for the optimization of many experimental situations.

Hopefully, the knowledge brought by this chapter can motivate the readers to see the usefulness of the factorial design of experiments and encourage them to apply this knowledge to their own experimental situations.

Table 21 List of papers related to materials synthesis and characterization

Experimental situation and year of publication	Factorial design	RSM	Goal	Refs.
Synthesis of Ag nanoparticles using plant extract, 2020	N/A	CCD for 5 factors	Maximize the intensity of SPR peak	[26]
Synthesis of AgInS ₂ /ZnS in aqueous media using microwave heating, 2020	2 ⁵⁻¹	2 ³ -CCD	Photoluminescence emission peak and lifetime, quantum yield, and Ag:In:Zn ratio	[27]
Functionalization of amino-silane on superparamagnetic iron oxide nanoparticles, 2020	N/A	2 ² -CCD	Atomic percentage of Fe, N, and Si	[28]
Synthesis of Au nanoparticles using <i>Coffea arabica</i> extract, 2019	2 ⁵⁻¹	3 ²	Maximize yield, monodispersity, control shape and size	[29]
Synthesis of ZrO ₂ nanoparticles using plant extract, 2019	2 ³ with replicas in central point	N/A	Maximize the amount of tetracycline adsorbed in ZrO ₂ . Maximize the percentage of tetragonal ZrO ₂ phase. Particle size control	[30]
Synthesis of Ni ₂ P in phosphonium-based ionic liquid, 2019	2 ⁶⁻³	DD	Control particle size	[31]
Synthesis of Au nanoparticles using plant extract by sonochemical method, 2019	N/A	CCD for 4 factors, and 5 levels per factor	Control de hydrodynamical size	[32]
Synthesis of CdSe quantum dots in aqueous media, 2019	2 ⁴ with central point	DD for 4 factors	Photoluminescence peak intensity and FWHM	[33]
Synthesis of Carbon quantum dots from chitin, chitosan, and graphite via hydrothermal carbonization, 2019	N/A	3 ²	Determination of quantum dot composition and band gap	[34]

(continued)

Table 21 (continued)

Experimental situation and year of publication	Factorial design	RSM	Goal	Refs.
Synthesis of iron oxide nanoparticles from mineral coal tailings, 2019	2^2 with central point	N/A	Control particle size	[35]
Synthesis of cyano-functionalized SiO ₂ nanoparticles, 2018	2^{6-2}	N/A	Minimize particle size and get narrow particle size distribution	[36]
Synthesis of 1-dimensional TiO ₂ via hydrothermal method, 2018	N/A	3^3 -BBD	Control the band gap energy and crystalline phases	[37]
Synthesis of multi-wall carbon nanotubes by chemical vapor deposition, 2018	2^4	N/A	Control the yield, band gap and aspect ratio of the carbon nanotubes	[38]
Growth of highly oriented Sb ₂ Te ₃ thin-films by radio frequency sputtering, 2018	2^{5-1} with replicas in central point	BBD	Maximize the degree of thin-film preferred growth	[39]
Synthesis of SrMoO ₄ using EDTA-Citrate complexation method, 2018	2^3 with replicas in central point	N/A	Control SrMoO ₄ band gap	[40]
Synthesis of Au nanorods by reduction with NaBH ₄ and ascorbic acid, 2017	2^{8-4}	CCD	Control SPR peak, particle dimensions and distribution, yield, and shape purity	[41]
Synthesis of thiol-capped CdTe quantum dots using microwave heating, 2017	N/A	2^3 -CCD	Maximize photoluminescence quantum yield	[42]
Electrodeposition of Cu ₂ O thin-films by tuning morphology and optical properties, 2017	2^4	N/A	Deposition charge and morphology coverage degree	[43]
Synthesis of ZnO by coprecipitation in aqueous media, 2017	2^3	N/A	Control the crystallite size	[44]

(continued)

Table 21 (continued)

Experimental situation and year of publication	Factorial design	RSM	Goal	Refs.
Synthesis of curcumin-loaded albumin nanoparticles at room temperature, 2017	2 ⁴	N/A	Control particle size, yield, and drug loading	[45]

Abbreviations: *BBD* Box-Behnken Design, *CCD* = central composite design, *DD* = Doehlert Design, *EDTA* = Ethylenediaminetetraacetic acid

Table 22 List of papers related to drug encapsulation and delivery

Experimental situation and year of publication	Factorial design	RSM	Goal	Refs.
Design of SLN as nanocarrier for the anticancer drug docetaxel, 2019	2 ³ with replicas in central point	N/A	Control hydrodynamic diameter, polydispersity index, and zeta potential	[46]
Design of curcumin-loaded SLN for inhibition of post-angioplasty restenosis, 2019	2 ⁴ with replicas in central point	N/A	Control entrapment efficiency, hydrodynamic diameter, polydispersity index, and zeta potential	[47]
Design of antiretroviral drug ritonavir-loaded SLN, 2019	N/A	3 ²	Particle size minimization, entrapment efficiency and zeta potential maximization	[48]
Design of PLGA nanoparticles for co-delivery of temozolomide and O6-benzylguanine. 2019	2 ⁵⁻² with replicas in central point	N/A	Control entrapment efficiency, hydrodynamic diameter, polydispersity index, and zeta potential	[49]
Design of furosemide loaded SLN, 2018	N/A	3 ²	Entrapment and dissolution efficiencies maximization; particle size, polydispersity index, and time elapsed for 50% drug release minimization	[50]

(continued)

Table 22 (continued)

Experimental situation and year of publication	Factorial design	RSM	Goal	Refs.
Design of PLGA-chitosan nanoparticles loaded with a HIV-1 fusion inhibitor peptide, 2018	N/A	2^3 - CCD	Control entrapment efficiency, polydispersity index, and average particle size	[51]
Design of HSA nanoparticle for entrapment of anticancer agent irinotecan, 2018	N/A	3^2	Control entrapment efficiency, polydispersity index, particle size, and drug loading percentage	[52]
Design of chitosan-based nanogels for controlled release of the antibiotic gentamicin, 2018	2^{8-2} with replicas in central point	CCD	Control particle size and loading efficiency	[53]
Design of poly-caprolactone nanoparticles loaded with the antipsychotics olanzapine, 2018	N/A	3^2	Control particle size and encapsulation efficiency	[54]
Design of octanoyl chitosan nanoparticles for improved rifampicin pulmonary delivery, 2018	N/A	3^2	Particle size minimization and entrapment efficiency minimization	[55]
Design of SLN loaded with the anti-cancer drug citral, 2018	2^2 with replicas in central point	N/A	Control mean particle size, polydispersity index, and zeta potential	[56]
Design of PLGA loaded with the anti-cancer drug doxorubicin, 2017	N/A	BBD	Particle size, polydispersity index, and zeta potential minimization; entrapment efficiency maximization	[57]
Design of SLN of efavirenz for brain targeting and enhanced availability, 2017	N/A	3^2	Control mean particle size, polydispersity index, and entrapment efficiency	[58]
Design of multiple protein delivery for cardiac repair, 2016	2^{4-1}	N/A	Determine the ejection efficiency	[59]
Design of curcumin-loaded PLGA nanoparticles for colon delivery, 2016	2^3	N/A	Control particle size, zeta potential, entrapment efficiency, and in vitro release over 24 h	[60]

(continued)

Table 22 (continued)

Experimental situation and year of publication	Factorial design	RSM	Goal	Refs.
Design of levofloxacin-loaded stearic acid SLN for ocular delivery, 2016	N/A	BBD with 3 factors and 3 levels	Control particle size and entrapment efficiency	[61]
Design of PLGA/poloxamer nanoparticles loaded with zolmitriptan, 2016	2 ⁴	N/A	Control particle size, entrapment efficiency, and cumulative drug release in 8 h	[62]
Design of carvedilol-load SLN for intranasal drug delivery, 2016	2 ³	N/A	Control particle size, entrapment efficiency, and amount of drug permeated per unit area in 24 h	[63]
Design of paclitaxel-loaded folate-conjugated amphiphilic cyclodextrin nanoparticles, 2016	N/A	3 ²	Control particle size, polydispersity index, entrapment efficiency, zeta potential, and paclitaxel amount per polymer	[64]
Design of methotrexate-loading in chitosan nanoparticles, 2016	N/A	3 ²	Control particle size, polydispersity index, entrapment efficiency, and zeta potential	[65]

Abbreviations: *BBD* Box-Behnken Design, *CCD* central composite design, *HAS* human serum albumin, *PLGA* poly(D,L-lactic-co-glycolic acid), *SLN* solid lipid nanoparticles

Table 23 List of papers related to wastewater remediation

Experimental situation and year of publication	Factorial design	RSM	Goal	Refs.
Removal of the dye tartrazine by UV-light photocatalytic degradation using zinc oxide (ZnO) nanorods with different aspect ratios, 2020	2 ⁴	N/A	Maximize removal efficiency and pseudo-first-order rate constant	[66]
Central composite design to mineralization of olive mill wastewater by the electro/Fe ⁺² /persulfate oxidation method, 2020	N/A	2 ³ -CCD	Decrease chemical oxygen demand in olive mill wastewater	[67]

(continued)

Table 23 (continued)

Experimental situation and year of publication	Factorial design	RSM	Goal	Refs.
Electrocoagulation for treating Kraft paper mill wastewater, 2020	N/A	2 ² -CCD	Maximize the removal efficiency of color, chemical oxygen demand, biochemical oxygen demand, and tannin/lignin ratio. Also to maximize the biodegradability index	[68]
Microplastic pollution reduction by a carbon and nitrogen-doped TiO ₂ via visible light photocatalytic degradation, 2020	2 ² with replicas in central point	N/A	Maximize high density polyethylene mass loss in microplastics	[69]
Removal of nickel and COD from wastewater from electroplating industry using Electrocoagulation and AOP, 2020	2 ³	Multiple 2 ² designs until finding the optimum value for each level	Maximize the removal efficiency and COD from wastewater from electroplating industry	[70]
Pesticide Diuron removal from wastewater by photo-electrochemical oxidation with TiO ₂ Nanotubes, 2020	2 ³	N/A	Maximize the specific rate of removal and minimize the cell potential	[71]
Graphene oxide/TiO ₂ for visible light photocatalysis to degrade eight pharmaceutical contaminants from water and wastewater, 2020	N/A	BBD with three factors	Maximize the mineralization percentage of the pharmaceutical contaminants	[72]
Solar electrocoagulation and adsorption processes with granular oil palm shell activated carbon for Pb(II) removal from aqueous solution, 2019	N/A	2 ³ -CCD	Maximize the removal efficiency	[73]
Performance of different coagulants in the coagulation/flocculation process of textile wastewater, 2019	N/A	3 ²	Analyze the chemical oxygen demand of the coagulation/flocculation process	[74]
Electrodisinfection of real swine wastewater for water reuse, 2019	2 ²	N/A	Maximize <i>E. coli</i> inactivation	[75]

(continued)

Table 23 (continued)

Experimental situation and year of publication	Factorial design	RSM	Goal	Refs.
L-Histidine (C, N) codoped-TiO ₂ -CdS nanocomposite for efficient visible photo-degradation of recalcitrant compounds from wastewater, 2019	N/A	CCD	Maximize methyl orange removal efficiency	[76]
Optimization of saline wastewater treatment using electrochemical oxidation process, 2019	N/A	2 ⁴ -CCD	Maximize COD and TOC removal from saline wastewaters using electrochemical oxidation process	[77]
Biological treatment of wastewater containing a mixture of polycyclic aromatic hydrocarbons using the oleaginous bacterium <i>Rhodococcus opacus</i> , 2018	2 ³	N/A	Maximize polycyclic aromatic hydrocarbons removal efficiency	[78]
Degradation of paracetamol by an UV/Chlorine advanced oxidation process, 2018	N/A	2 ⁴ -CCD	Maximize paracetamol removal efficiency	[79]
Electrochemical treatment of wastewater from a bakery industry, 2018	2 ³	N/A	Maximize removal of COD and minimize turbidity	[80]
Sono-photo-Fenton process for degradation of phenol derivatives in petrochemical wastewater, 2018	N/A	3 ³	Maximize the removal of COD	[81]
Decolorization of Reactive Blue 235 dye by barium alginate immobilized iron nanoparticles synthesized from aluminum industry waste, 2017	N/A	BBD with 4 factors and 3 levels	Maximize the Reactive Blue 235 removal efficiency	[82]
Carbon and CNT fabricated carbon substrates for TiO ₂ nanoparticles immobilization for continuous photocatalytic elimination of dye molecules, 2017	N/A	2 ⁴ -CCD	Maximize the dye and COD removal efficiency, and minimize electrical energy consumption	[83]

(continued)

Table 23 (continued)

Experimental situation and year of publication	Factorial design	RSM	Goal	Refs.
Evaluation and disposability study of actual textile wastewater treatment by electro-oxidation method using Ti/RuO ₂ anode, 2017	N/A	BBD with 3 factors and 3 levels	Maximize the color and COD removal efficiency, and minimize electrical energy consumption	[84]
Treatment of real wastewater with TiO ₂ -films sensitized by a natural-dye obtained from <i>Picramnia sellowii</i> , 2016	2 ³	N/A	Maximize the color and COD removal efficiency	[85]

Abbreviations: *AOP* advanced oxidative process, *BBD* Box-Behnken Design, *CCD* central composite design, *CNT* carbon nanotubes, *COD* chemical oxygen demand, *TOC* total organic carbon

Table 24 List of papers related to solar cells design and performance

Experimental situation and year of publication	Factorial design	RSM	Goal	Refs.
Doping of polyaniline to prepare polymer electrolytes for DSSC, 2020	N/A	3 ²	Increase the efficiency of the DSSC	[86]
Improving the properties of indium tin oxide thin films by the incorporation of carbon nanotubes with solution-based techniques, 2020	2 ³	N/A	Minimize the sheet resistance of the thin-film	[87]
Optimization and performance analysis of a solar concentrated photovoltaic-thermoelectric hybrid system, 2020	N/A	2 ⁴ -CCD	Increase the electrical efficiency of the solar concentrated photovoltaic-thermoelectric hybrid system	[88]
Ga-doped indium-zinc oxide films obtained by magnetron sputtering as transparent conductors for visible and solar applications, 2019	N/A	BBD	Control the chemical composition, optical, electrical, and structural properties of the GIZO film	[89]

(continued)

Table 24 (continued)

Experimental situation and year of publication	Factorial design	RSM	Goal	Refs.
Optimizing the optical properties of a dye-based luminescent down-shifter to improve the performance of organic photovoltaic devices, 2019	2 ³ with replicas	N/A	Control the absorbance and photoluminescence quantum yield	[90]
Multistress testing of OPV modules for accurate predictive aging and reliability predictions, 2018	2 ³	N/A	Study the degradation to 80% or 50% of the original maximum efficiency value	[91]
Improve the properties of Cu ₂ ZnSnS ₄ films grown by spray pyrolysis, 2017	N/A	2 ³ -CCD	Improve the microstructural properties of Cu ₂ ZnSnS ₄ films	[92]
Modeling of organic solar cell using response surface methodology, 2017	N/A	2 ³ -CCD	Improve the organic solar cell performance	[93]
Systematic optimization of boron diffusion for solar cell emitters, 2017	2 ⁴	N/A	Control sheet resistance, lifetime, surface concentration, and junction depth of the solar cell emitter	[94]
Modeling of photogenerated charge collection of silver-based plasmonic DSSC using CCD experiments, 2017	N/A	2 ⁵ -CCD	Improve the charge collection	[95]
Systematic optimization of phosphorous diffusion for solar cell application, 2016	2 ⁵	N/A	Control the sheet resistance, lifetime, and junction depth of solar cell p-n junction	[96]
XPS analysis of the chemical degradation of PTB7 polymers for organic photovoltaics, 2016	2 ³	N/A	Control the stability of the PTB7 polymer	[97]

Abbreviations: *BBD* Box-Behnken Design, *CCD* central composite design, *DSSC* dye-sensitized solar cell, *PTB7* Poly[[4,8-bis[(2-ethylhexyl)oxy]benzo[1,2-b:4,5-b']dithiophene-2,6-diy]]-[3-fluoro-2-[(2-ethylhexyl)carbonyl]thieno[3,4-b]thio-phenediyl]], *OPV* organic photovoltaic

Acknowledgements The author would like to thank Manhattan College for support through startup funds and Faculty Summer Grant. The author gently dedicates this chapter to his family Olavio, Evanilde, Maria, Daniel, Caroline, Anthony, and Brianne.

References

1. Neto, B.B., Scarmino, I.S., Bruns, R.E.: *Como Fazer Experimentos - Pesquisa e Desenvolvimento na Ciência e na Indústria*, 4th ed., Bookman (2010)
2. Montgomery, D.C.: Experimental design for product and process design and development. *J. R. Stat. Soc. Ser. D (The Stat.)* **48**, 159–177 (1999). <https://doi.org/10.1111/1467-9884.00179>
3. Lundstedt, T., Seifert, E., Abramo, L., Thelin, B., Nyström, Å., Pettersen, J., Bergman, R.: Experimental design and optimization. *Chemom. Intell. Lab. Syst.* **42**, 3–40 (1998). [https://doi.org/10.1016/S0169-7439\(98\)00065-3](https://doi.org/10.1016/S0169-7439(98)00065-3)
4. Pereira, F., Pereira-Filho, E.: Aplicação de programa computacional livre em planejamento de experimentos: um tutorial. *Quim. Nova.* 1061–1071 (2018). <https://doi.org/10.21577/0100-4042.20170254>
5. Vera Candiotti, L., De Zan, M.M., Cámara, M.S., Goicoechea, H.C.: Experimental design and multiple response optimization. Using the desirability function in analytical methods development. *Talanta* **124**, 123–138 (2014). <https://doi.org/10.1016/j.talanta.2014.01.034>
6. Mee, R.W.: *A Comprehensive Guide to Factorial Two-Level Experimentation*. Springer (2009)
7. Hibbert, D.B.: Experimental design in chromatography: a tutorial review. *J. Chromatogr. B Anal. Technol. Biomed. Life Sci.* **910**, 2–13 (2012). <https://doi.org/10.1016/j.jchromb.2012.01.020>
8. Ferreira, S.L.C., Lemos, V.A., de Carvalho, V.S., da Silva, E.G.P., Queiroz, A.F.S., Felix, C.S.A., da Silva, D.L.F., Dourado, G.B., Oliveira, R.V.: Multivariate optimization techniques in analytical chemistry—an overview. *Microchem. J.* **140**, 176–182 (2018). <https://doi.org/10.1016/j.microc.2018.04.002>
9. Teófilo, R.F., Ferreira, M.M.C.: Quimiometria II: planilhas eletrônicas para cálculos de planejamentos experimentais, um tutorial. *Quim. Nova.* **29**, 338–350 (2006). <https://doi.org/10.1590/S0100-40422006000200026>
10. Dean, A., Voss, D., Draguljić, D.: *Design and Analysis of Experiments*, 2nd ed. Springer International Publishing, Cham (2017). <https://doi.org/10.1007/978-3-319-52250-0>
11. Novaes, C.G., Bezerra, M.A., da Silva, E.G.P., dos Santos, A.M.P., Romão, I.L.S., Santos Neto, J.H.: A review of multivariate designs applied to the optimization of methods based on inductively coupled plasma optical emission spectrometry (ICP OES). *Microchem. J.* **128**, 331–346 (2016). <https://doi.org/10.1016/j.microc.2016.05.015>
12. Ferreira, S.L.C., Dos Santos, W.N.L., Quintella, C.M., Neto, B.B., Bosque-Sendra, J.M.: Doehlert matrix: a chemometric tool for analytical chemistry—review. *Talanta* **63**, 1061–1067 (2004). <https://doi.org/10.1016/j.talanta.2004.01.015>
13. Pasma, S.A., Daik, R., Maskat, M.Y., Hassan, O.: Application of box-behnken design in optimization of glucose production from oil palm empty fruit bunch cellulose. *Int. J. Polym. Sci.* (2013). <https://doi.org/10.1155/2013/104502>
14. Ferreira, S.L.C., Bruns, R.E., Ferreira, H.S., Matos, G.D., David, J.M., Brandão, G.C., da Silva, E.G.P., Portugal, L.A., dos Reis, P.S., Souza, A.S., dos Santos, W.N.L.: Box-Behnken design: an alternative for the optimization of analytical methods. *Anal. Chim. Acta.* **597**, 179–186 (2007). <https://doi.org/10.1016/j.aca.2007.07.011>
15. Ferreira, S.L.C., Silva Junior, M.M., Felix, C.S.A., da Silva, D.L.F., Santos, A.S., Santos Neto, J.H., de Souza, C.T., Cruz Junior, R.A., Souza, A.S.: Multivariate optimization techniques in food analysis—a review. *Food Chem.* **273**, 3–8 (2019). <https://doi.org/10.1016/j.foodchem.2017.11.114>
16. Granata, G., Yamaoka, T., Pagnanelli, F., Fuwa, A.: Study of the synthesis of copper nanoparticles: the role of capping and kinetic towards control of particle size and stability. *J. Nanoparticle Res.* **18**, 1–12 (2016). <https://doi.org/10.1007/s11051-016-3438-6>
17. Masalov, V.M., Sukhinina, N.S., Kudrenko, E.A., Emelchenko, G.A.: Mechanism of formation and nanostructure of Stöber silica particles. *Nanotechnology* **22** (2011). <https://doi.org/10.1088/0957-4484/22/27/275718>

18. Hartlen, K.D., Athanasopoulos, A.P.T., Kitaev, V.: Facile preparation of highly monodisperse small silica spheres (15 to >200 nm) suitable for colloidal templating and formation of ordered arrays. *Langmuir* **24**, 1714–1720 (2008). <https://doi.org/10.1021/la7025285>
19. Arantes, T.M., Pinto, A.H., Leite, E.R., Longo, E., Camargo, E.R.: Synthesis and optimization of colloidal silica nanoparticles and their functionalization with methacrylic acid. *Colloids Surf. Physicochem. Eng. Asp.* **415** (2012). <https://doi.org/10.1016/j.colsurfa.2012.09.041>
20. Hannachi, A., Hammami, S., Raouafi, N., Maghraoui-Meherzi, H.: Preparation of manganese sulfide (MnS) thin films by chemical bath deposition: application of the experimental design methodology. *J. Alloys Compd.* **663**, 507–515 (2016). <https://doi.org/10.1016/j.jallcom.2015.11.058>
21. Dahl, J.A., Maddux, B.L.S., Hutchison, J.E.: Toward greener nanosynthesis. *Chem. Rev.* **107**, 2228–2269 (2007). <https://doi.org/10.1021/cr050943k>
22. Martins, L.R., Rodrigues, J.A.V., Adarme, O.F.H., Melo, T.M.S., Gurgel, L.V.A., Gil, L.F.: Optimization of cellulose and sugarcane bagasse oxidation: application for adsorptive removal of crystal violet and auramine-O from aqueous solution. *J. Colloid Interface Sci.* **494**, 223–241 (2017). <https://doi.org/10.1016/j.jcis.2017.01.085>
23. Rafique, M., Sadaf, I., Rafique, M.S., Tahir, M.B.: A review on green synthesis of silver nanoparticles and their applications. *Artif. Cells, Nanomed. Biotechnol.* **45**, 1272–1291 (2017). <https://doi.org/10.1080/21691401.2016.1241792>
24. Núñez, R.N., Veglia, A.V., Pacioni, N.L.: Improving reproducibility between batches of silver nanoparticles using an experimental design approach. *Microchem. J.* **141**, 110–117 (2018). <https://doi.org/10.1016/j.microc.2018.05.017>
25. Eising, R., Signori, A.M., Fort, S., Domingos, J.B.: Development of catalytically active silver colloid nanoparticles stabilized by dextran. *Langmuir* **27**, 11860–11866 (2011). <https://doi.org/10.1021/la2029164>
26. Nikaeen, G., Yousefinejad, S., Rahmdel, S., Samari, F., Mahdavinia, S.: Central composite design for optimizing the biosynthesis of silver nanoparticles using plantago major extract and investigating antibacterial, antifungal and antioxidant activity. *Sci. Rep.* **10**, 1–16 (2020). <https://doi.org/10.1038/s41598-020-66357-3>
27. Soares, J.X., Wegner, K.D., Ribeiro, D.S.M., Melo, A., Häusler, I., Santos, J.L.M., Resch-Genger, U.: Rationally designed synthesis of bright AgInS₂/ZnS quantum dots with emission control. *Nano Res.* **12** (2020). <https://doi.org/10.1007/s12274-020-2876-8>
28. Sodipo, B.K., Aziz, A.A.: Optimization of sonochemical method of functionalizing amino-silane on superparamagnetic iron oxide nanoparticles using central composite design. *Ultrason. Sonochem.* **64**, 104856 (2020). <https://doi.org/10.1016/j.ultsonch.2019.104856>
29. Keijok, W.J., Pereira, R.H.A., Alvarez, L.A.C., Prado, A.R., da Silva, A.R., Ribeiro, J., de Oliveira, J.P., Guimarães, M.C.C.: Controlled biosynthesis of gold nanoparticles with *Coffea arabica* using factorial design. *Sci. Rep.* **9**, 1–10 (2019). <https://doi.org/10.1038/s41598-019-52496-9>
30. da Silva, A.F.V., Fagundes, A.P., Macuvele, D.L.P., de Carvalho, E.F.U., Durazzo, M., Padoin, N., Soares, C., Riella, H.G.: Green synthesis of zirconia nanoparticles based on *Euclea natalensis* plant extract: optimization of reaction conditions and evaluation of adsorptive properties. *Colloids Surf. Physicochem. Eng. Asp.* **583**, 123915 (2019). <https://doi.org/10.1016/j.colsurfa.2019.123915>
31. Mora-Tamez, L., Barim, G., Downes, C., Williamson, E.M., Habas, S.E., Brutchey, R.L.: Controlled design of phase- and size-tunable monodisperse Ni₂P nanoparticles in a phosphonium-based ionic liquid through response surface methodology. *Chem. Mater.* **31**, 1552–1560 (2019). <https://doi.org/10.1021/acs.chemmater.8b04518>
32. Usman, A.I., Aziz, A.A., Sodipo, B.K.: Application of central composite design for optimization of biosynthesized gold nanoparticles via sonochemical method. *SN Appl. Sci.* **1**, 1–9 (2019). <https://doi.org/10.1007/s42452-019-0429-0>
33. Viegas, I.M.A., Santos, B.S., Fontes, A., De Lima Pereira, G.A., Pereira, C.F.: Multivariate optimization of optical properties of CdSe quantum dots obtained by a facile one-pot aqueous synthesis. *Inorg. Chem. Front.* **6**, 1350–1360 (2019). <https://doi.org/10.1039/c9qi00105k>

34. Gomes, M.F., Gomes, Y.F., Lopes-Moriyama, A., de Barros Neto, E.L., de Souza, C.P.: Design of carbon quantum dots via hydrothermal carbonization synthesis from renewable precursors. *Biomass Convers. Biorefinery* **9**, 689–694 (2019). <https://doi.org/10.1007/s13399-019-00387-4>
35. Maass, D., Valério, A., Lourenço, L.A., de Oliveira, D., Hotza, D.: Biosynthesis of iron oxide nanoparticles from mineral coal tailings in a stirred tank reactor. *Hydrometallurgy* **184**, 199–205 (2019). <https://doi.org/10.1016/j.hydromet.2019.01.010>
36. Elazazy, M.S., Issa, A.A., Al-Mashreky, M., Al-Sulaiti, M., Al-Saad, K.: Application of fractional factorial design for green synthesis of cyano-modified silica nanoparticles: chemometrics and multifarious response optimization. *Adv. Powder Technol.* **29**, 1204–1215 (2018). <https://doi.org/10.1016/j.apt.2018.02.012>
37. Peng, T., Ray, S., Veeravalli, S.S., Lalman, J.A., Arefi-Khonsari, F.: The role of hydrothermal conditions in determining 1D TiO₂ nanomaterials bandgap energies and crystal phases. *Mater. Res. Bull.* **105**, 104–113 (2018). <https://doi.org/10.1016/j.materresbull.2018.04.021>
38. Obasogie, O.E., Abdulkareem, A.S., Mohammed, I.A., Bankole, M.T., Tijani, J.O., Abubakre, O.K.: Empirical relationship between band gap and synthesis parameters of chemical vapor deposition-synthesized multiwalled carbon nanotubes. *Carbon Lett.* **28**, 72–80 (2018). <https://doi.org/10.5714/CL.2018.28.072>
39. Behera, J.K., Zhou, X., Ranjan, A., Simpson, R.E.: Sb₂Te₃ and its superlattices: optimization by statistical design. *ACS Appl. Mater. Interf.* **10**, 15040–15050 (2018). <https://doi.org/10.1021/acsami.8b02100>
40. Silva, M.M.S., Sena, M.S., Lopes-Moriyama, A.L., Souza, C.P., Santos, A.G.: Experimental planning of the synthesis of strontium molybdate by EDTA-citrate and its structural influence, morphology and optical bandgap. *Ceram. Int.* **44**, 16606–16614 (2018). <https://doi.org/10.1016/j.ceramint.2018.06.087>
41. Burrows, N.D., Harvey, S., Idesis, F.A., Murphy, C.J.: Understanding the seed-mediated growth of gold nanorods through a fractional factorial design of experiments. *Langmuir* **33**, 1891–1907 (2017). <https://doi.org/10.1021/acs.langmuir.6b03606>
42. Ribeiro, D.S.M., de Souza, G.C.S., Melo, A., Soares, J.X., Rodrigues, S.S.M., Araújo, A.N., Montenegro, M.C.B.S.M., Santos, J.L.M.: Synthesis of distinctly thiol-capped CdTe quantum dots under microwave heating: multivariate optimization and characterization. *J. Mater. Sci.* **52**, 3208–3224 (2017). <https://doi.org/10.1007/s10853-016-0610-4>
43. Cembrero-Coca, P., Cembrero, J., Busquets-Mataix, D., Pérez-Puig, M.A., Marí, B., Pruna, A.: Factorial electrochemical design for tailoring of morphological and optical properties of Cu₂O. *Mater. Sci. Technol. (United Kingdom)* **33**, 2102–2109 (2017). <https://doi.org/10.1080/02670836.2017.1349595>
44. Machado, M.M., Savi, B.M., Perucchi, M.B., Benedetti, A., Oliveira, L.F.S., Bernardin, A.M.: Effect of temperature, precursor type and dripping time on the crystallite size of nano ZnO obtained by one-pot synthesis: 2 k full factorial design analysis. *J. Nanosci. Nanotechnol.* **18**, 4409–4412 (2017). <https://doi.org/10.1166/jnn.2018.15043>
45. Safavi, M.S., Shojaosadati, S.A., Yang, H.G., Kim, Y., Park, E.J., Lee, K.C., Na, D.H.: Reducing agent-free synthesis of curcumin-loaded albumin nanoparticles by self-assembly at room temperature. *Int. J. Pharm.* **529**, 303–309 (2017). <https://doi.org/10.1016/j.ijpharm.2017.06.087>
46. Albano, J.M.R., Ribeiro, L.N.M., Couto, V.M., Barbosa Messias, M., Rodrigues da Silva, G.H., Breikreitz, M.C., de Paula, E., Pickholz, M.: Rational design of polymer-lipid nanoparticles for docetaxel delivery. *Colloids Surf. B Biointerf.* **175**, 56–64 (2019). <https://doi.org/10.1016/j.colsurfb.2018.11.077>
47. Akhlaghi, S., Rabbani, S., Alavi, S., Alinaghi, A., Radfar, F., Dadashzadeh, S., Haeri, A.: Green formulation of curcumin loaded lipid-based nanoparticles as a novel carrier for inhibition of post-angioplasty restenosis. *Mater. Sci. Eng. C.* **105**, 110037 (2019). <https://doi.org/10.1016/j.msec.2019.110037>
48. Pavan Rudhratla, V.S.A., Sudhakar, B., Suresh Reddy, K.V.N.: Ritonavir loaded surface modified stealth solid lipid nanoparticles: full factorial design and pharmacokinetic studies. *Int. J. Res. Pharm. Sci.* **10**, 77–89 (2019). <https://doi.org/10.26452/ijrps.v10i1.1783>

49. Ramalho, M.J., Loureiro, J.A., Coelho, M.A.N., Pereira, M.C.: Factorial design as a tool for the optimization of p1ga nanoparticles for the co-delivery of temozolomide and o6-benzylguanine. *Pharmaceutics* **11** (2019). <https://doi.org/10.3390/pharmaceutics11080401>
50. Ali, H., Singh, S.K.: Preparation and characterization of solid lipid nanoparticles of furosemide using quality by design. *Part. Sci. Technol.* **36**, 695–709 (2018). <https://doi.org/10.1080/02726351.2017.1295293>
51. Ariza-Sáenz, M., Espina, M., Calpena, A., Gómara, M.J., Pérez-Pomeda, I., Haro, I., García, M.L.: Design, characterization, and biopharmaceutical behavior of nanoparticles loaded with an HIV-1 fusion inhibitor peptide. *Mol. Pharm.* **15**, 5005–5018 (2018). <https://doi.org/10.1021/acs.molpharmaceut.8b00609>
52. Taneja, N., Singh, K.K.: Rational design of polysorbate 80 stabilized human serum albumin nanoparticles tailored for high drug loading and entrapment of irinotecan. *Int. J. Pharm.* **536**, 82–94 (2018). <https://doi.org/10.1016/j.ijpharm.2017.11.024>
53. Zabihian, A., Salouti, M., Hamidi, M.: Factorial design analysis and optimisation of chitosan-based nanogels as controlled release system for gentamicin. *IET Nanobiotechnol.* **12**, 12–17 (2018). <https://doi.org/10.1049/iet-nbt.2017.0114>
54. Joseph, E., Reddi, S., Rinwa, V., Balwani, G., Saha, R.: DoE based Olanzapine loaded polycaprolactone nanoparticles decreases extrapyramidal effects in rodent model. *Int. J. Pharm.* **541**, 198–205 (2018). <https://doi.org/10.1016/j.ijpharm.2018.02.010>
55. Petkar, K.C., Chavhan, S., Kunda, N., Saleem, I., Somavarapu, S., Taylor, K.M.G., Sawant, K.K.: Development of novel octanoyl chitosan nanoparticles for improved rifampicin pulmonary delivery: optimization by factorial design. *AAPS Pharm. Sci. Tech.* **19**, 1758–1772 (2018). <https://doi.org/10.1208/s12249-018-0972-9>
56. Zielińska, A., Martins-Gomes, C., Ferreira, N.R., Silva, A.M., Nowak, I., Souto, E.B.: Anti-inflammatory and anti-cancer activity of citral: optimization of citral-loaded solid lipid nanoparticles (SLN) using experimental factorial design and LUMiSizer®. *Int. J. Pharm.* **553**, 428–440 (2018). <https://doi.org/10.1016/j.ijpharm.2018.10.065>
57. Shaikh, M.V., Kala, M., Nivsarkar, M.: Formulation and optimization of doxorubicin loaded polymeric nanoparticles using Box-Behnken design: ex-vivo stability and in-vitro activity. *Eur. J. Pharm. Sci.* **100**, 262–272 (2017). <https://doi.org/10.1016/j.ejps.2017.01.026>
58. Gupta, S., Kesarla, R., Chotai, N., Misra, A., Omri, A.: Systematic approach for the formulation and optimization of solid lipid nanoparticles of efavirenz by high pressure homogenization using design of experiments for brain targeting and enhanced bioavailability. *Biomed Res. Int.* (2017). <https://doi.org/10.1155/2017/5984014>
59. Awada, H.K., Johnson, L.A., Hitchens, T.K., Foley, L.M., Wang, Y.: Factorial design of experiments to optimize multiple protein delivery for cardiac repair. *ACS Biomater. Sci. Eng.* **2**, 879–886 (2016). <https://doi.org/10.1021/acsbiomaterials.6b00146>
60. Akl, M.A., Kartal-Hodzic, A., Oksanen, T., Ismael, H.R., Afouna, M.M., Yliperttula, M., Samy, A.M., Viitala, T.: Factorial design formulation optimization and in vitro characterization of curcumin-loaded PLGA nanoparticles for colon delivery. *J. Drug Deliv. Sci. Technol.* **32**, 10–20 (2016). <https://doi.org/10.1016/j.jddst.2016.01.007>
61. Baig, M.S., Ahad, A., Aslam, M., Imam, S.S., Aqil, M., Ali, A.: Application of Box-Behnken design for preparation of levofloxacin-loaded stearic acid solid lipid nanoparticles for ocular delivery: optimization, in vitro release, ocular tolerance, and antibacterial activity. *Int. J. Biol. Macromol.* **85**, 258–270 (2016). <https://doi.org/10.1016/j.ijbiomac.2015.12.077>
62. Girotra, P., Singh, S.K., Kumar, G.: Development of zolmitriptan loaded PLGA/poloxamer nanoparticles for migraine using quality by design approach. *Int. J. Biol. Macromol.* **85**, 92–101 (2016). <https://doi.org/10.1016/j.ijbiomac.2015.12.069>
63. Aboud, H.M., El komy, M.H., Ali, A.A., El Menshawe, S.F., Abd Elbary, A.: Development, optimization, and evaluation of carvedilol-loaded solid lipid nanoparticles for intranasal drug delivery. *AAPS Pharm. Sci. Tech.* **17**, 1353–1365 (2016). <https://doi.org/10.1208/s12249-015-0440-8>
64. Erdoğar, N., Esendağlı, G., Nielsen, T.T., Şen, M., Öner, L., Bilensoy, E.: Design and optimization of novel paclitaxel-loaded folate-conjugated amphiphilic cyclodextrin nanoparticles. *Int. J. Pharm.* **509**, 375–390 (2016). <https://doi.org/10.1016/j.ijpharm.2016.05.040>

65. Hashad, R.A., Ishak, R.A.H., Geneidi, A.S., Mansour, S.: Methotrexate loading in chitosan nanoparticles at a novel pH: response surface modeling, optimization and characterization. *Int. J. Biol. Macromol.* **91**, 630–639 (2016). <https://doi.org/10.1016/j.ijbiomac.2016.06.014>
66. Skinner, A.W., DiBernardo, A.M., Masud, A.M., Aich, N., Pinto, A.H.: Factorial design of experiments for optimization of photocatalytic degradation of tartrazine by zinc oxide (ZnO) nanorods with different aspect ratios. *J. Environ. Chem. Eng.* 104235 (2020). <https://doi.org/10.1016/j.jece.2020.104235>
67. Görmez, F., Görmez, Ö., Yabalak, E., Gözmen, B.: Application of the central composite design to mineralization of olive mill wastewater by the electro/FeII/persulfate oxidation method. *SN Appl. Sci.* **2**, 1–11 (2020). <https://doi.org/10.1007/s42452-020-1986-y>
68. Wagle, D., Lin, C.J., Nawaz, T., Shipley, H.J.: Evaluation and optimization of electrocoagulation for treating Kraft paper mill wastewater. *J. Environ. Chem. Eng.* **8**, 103595 (2020). <https://doi.org/10.1016/j.jece.2019.103595>
69. Ariza-Tarazona, M.C., Villarreal-Chiu, J.F., Hernández-López, J.M., Rivera De la Rosa, J., Barbieri, V., Siligardi, C., Cedillo-González, E.I.: Microplastic pollution reduction by a carbon and nitrogen-doped TiO₂: effect of pH and temperature in the photocatalytic degradation process. *J. Hazard. Mater.* **395**, 122632 (2020). <https://doi.org/10.1016/j.jhazmat.2020.122632>
70. Moersidik, S.S., Nugroho, R., Handayani, M., Kamilawati, Pratama, M.A.: Optimization and reaction kinetics on the removal of nickel and COD from wastewater from electroplating industry using electrocoagulation and advanced oxidation processes. *Heliyon* **6**, e03319 (2020). <https://doi.org/10.1016/j.heliyon.2020.e03319>
71. Vacca, A., Mais, L., Mascia, M., Usai, E.M., Palmas, S.: Design of experiment for the optimization of pesticide removal from wastewater by photo-electrochemical oxidation with tio2 nanotubes. *Catalysts* **10** (2020). <https://doi.org/10.3390/catal10050512>
72. Checa, M., Beltrán, F.J., Rivas, F.J., Cordero, E.: On the role of a graphene oxide/titania catalyst, visible LED and ozone in removing mixtures of pharmaceutical contaminants from water and wastewater. *Environ. Sci. Water Res. Technol.* (2020). <https://doi.org/10.1039/d0ew00276c>
73. Hussin, F., Aroua, M.K., Szlachta, M.: Combined solar electrocoagulation and adsorption processes for Pb(II) removal from aqueous solution. *Chem. Eng. Process. Process Intensif.* **143**, 107619 (2019). <https://doi.org/10.1016/j.cep.2019.107619>
74. Dotto, J., Fagundes-Klen, M.R., Veit, M.T., Palácio, S.M., Bergamasco, R.: Performance of different coagulants in the coagulation/flocculation process of textile wastewater. *J. Clean. Prod.* **208**, 656–665 (2019). <https://doi.org/10.1016/j.jclepro.2018.10.112>
75. Simas, A., Mores, R., Steffens, J., Dallago, R.M., Kunz, A., Michelon, W., Fongaro, G., Viancelli, A.: Electrodisinfection of real swine wastewater for water reuse. *Environ. Chem. Lett.* **17**, 495–499 (2019). <https://doi.org/10.1007/s10311-018-0782-z>
76. Zangeneh, H., Zinatizadeh, A.A., Zinadini, S., Feyzi, M., Rafiee, E., Bahnemann, D.W.: A novel L-Histidine (C, N) codoped-TiO₂-CdS nanocomposite for efficient visible photo-degradation of recalcitrant compounds from wastewater. *J. Hazard. Mater.* **369**, 384–397 (2019). <https://doi.org/10.1016/j.jhazmat.2019.02.049>
77. Darvishmotevalli, M., Zarei, A., Moradnia, M., Noorisepehr, M., Mohammadi, H.: Optimization of saline wastewater treatment using electrochemical oxidation process: prediction by RSM method. *MethodsX.* **6**, 1101–1113 (2019). <https://doi.org/10.1016/j.mex.2019.03.015>
78. Goswami, L., Manikandan, N.A., Dolman, B., Pakshirajan, K., Pugazhenth, G.: Biological treatment of wastewater containing a mixture of polycyclic aromatic hydrocarbons using the oleaginous bacterium *Rhodococcus opacus*. *J. Clean. Prod.* **196**, 1282–1291 (2018). <https://doi.org/10.1016/j.jclepro.2018.06.070>
79. Dao, Y.H., Tran, H.N., Tran-Lam, T.T., Pham, T.Q., Le, G.T.: Degradation of paracetamol by an UV/chlorine advanced oxidation process: influencing factors, factorial design, and intermediates identification. *Int. J. Environ. Res. Public Health.* **15** (2018). <https://doi.org/10.3390/ijerph15122637>
80. de Santana, M.M., Zanoelo, E.F., Benincá, C., Freire, F.B.: Electrochemical treatment of wastewater from a bakery industry: experimental and modeling study. *Process Saf. Environ. Prot.* **116**, 685–692 (2018). <https://doi.org/10.1016/j.psep.2018.04.001>

81. Shokri, A.: Application of Sono-photo-Fenton process for degradation of phenol derivatives in petrochemical wastewater using full factorial design of experiment. *Int. J. Ind. Chem.* **9**, 295–303 (2018). <https://doi.org/10.1007/s40090-018-0159-y>
82. Natarajan, E., Ponnaiah, G.P.: Optimization of process parameters for the decolorization of reactive blue 235 dye by barium alginate immobilized iron nanoparticles synthesized from aluminum industry waste. *Environ. Nanotechnol. Monit. Manag.* **7**, 73–88 (2017). <https://doi.org/10.1016/j.enmm.2017.01.002>
83. Pajootan, E., Rahimdokht, M., Arami, M.: Carbon and CNT fabricated carbon substrates for TiO₂ nanoparticles immobilization with industrial perspective of continuous photocatalytic elimination of dye molecules. *J. Ind. Eng. Chem.* **55**, 149–163 (2017). <https://doi.org/10.1016/j.jiec.2017.06.039>
84. Kaur, P., Kushwaha, J.P., Sangal, V.K.: Evaluation and disposability study of actual textile wastewater treatment by electro-oxidation method using Ti/RuO₂ anode. *Process Saf. Environ. Prot.* **111**, 13–22 (2017). <https://doi.org/10.1016/j.psep.2017.06.004>
85. Fernández, J.A., Suan, A., Ramírez, J.C., Robles, J., Salcedo, J.C., Pedroza, A.M., Daza, C.E.: Treatment of real wastewater with TiO₂-films sensitized by a natural-dye obtained from *Picramnia sellowii*. *J. Environ. Chem. Eng.* **4**, 2848–2856 (2016). <https://doi.org/10.1016/j.jece.2016.05.037>
86. Patni, N., Pillai, S.G.: Optimization of the doping of polyaniline via response surface method to prepare polymer electrolytes for dye sensitized solar cells. *J. Environ. Chem. Eng.* **8**, 103709 (2020). <https://doi.org/10.1016/j.jece.2020.103709>
87. Gökçeli, G., Karatepe, N.: Improving the properties of indium tin oxide thin films by the incorporation of carbon nanotubes with solution-based techniques. *Thin Solid Films* **697**, 137844 (2020). <https://doi.org/10.1016/j.tsf.2020.137844>
88. Rejeb, O., Shittu, S., Ghenai, C., Li, G., Zhao, X., Bettayeb, M.: Optimization and performance analysis of a solar concentrated photovoltaic-thermoelectric (CPV-TE) hybrid system. *Renew. Energy.* **152**, 1342–1353 (2020). <https://doi.org/10.1016/j.renene.2020.02.007>
89. Solís-Cortés, D., Navarrete-Astorga, E., Costa-Krämer, J.L., Salguero-Fernandez, J., Schrebler, R., Leinen, D., Dalchiele, E.A., Ramos-Barrado, J.R., Martín, F.: Ga-doped IZO films obtained by magnetron sputtering as transparent conductors for visible and solar applications. *Ceram. Int.* **45**, 5577–5587 (2019). <https://doi.org/10.1016/j.ceramint.2018.12.017>
90. Fernandes, R.V., Cordeiro Junior, N.A., Pardo Perdomo, A.D., Duarte, J.L., Laureto, E.: Optimizing the optical properties of a dye-based luminescent down-shifter to improve the performance of organic photovoltaic devices. *Dye. Pigment.* **169**, 1–6 (2019). <https://doi.org/10.1016/j.dyepig.2019.04.074>
91. Stoichkov, V., Kumar, D., Tyagi, P., Kettle, J.: Multistress testing of OPV modules for accurate predictive aging and reliability predictions. *IEEE J. Photovolt.* **8**, 1058–1065 (2018). <https://doi.org/10.1109/JPHOTOV.2018.2838438>
92. Ramírez, E.A., Ramírez, A., Gordillo, G.: Cu₂ZnSnS₄ films grown in one-step process by spray pyrolysis with improved properties. *Mater. Sci. Semicond. Process.* **67**, 110–117 (2017). <https://doi.org/10.1016/j.mssp.2017.05.024>
93. Suliman, R., Mitul, A.F., Mohammad, L., Djira, G., Pan, Y., Qiao, Q.: Modeling of organic solar cell using response surface methodology. *Results Phys.* **7**, 2232–2241 (2017). <https://doi.org/10.1016/j.rinp.2017.04.037>
94. Ebrahimi, P., Kolahdouz, M., Iraj, M., Ganjian, M., Aghababa, H., Asl-Soleimani, E., Radamson, H.H.: Systematic optimization of boron diffusion for solar cell emitters. *J. Electron. Mater.* **46**, 4236–4241 (2017). <https://doi.org/10.1007/s11664-017-5364-5>
95. Buda, S., Shafie, S., Rashid, S.A., Jaafar, H., Khalifa, A.: Response surface modeling of photo-generated charge collection of silver-based plasmonic dye-sensitized solar cell using central composite design experiments. *Results Phys.* **7**, 493–497 (2017). <https://doi.org/10.1016/j.rinp.2017.01.011>

96. Kermaniha, M., Kolahdouz, M., Manavizadeh, N., Aghababa, H., Elahi, M., Iraj, M., Asl-Soleimani, E., Radamson, H.H.: Systematic optimization of phosphorous diffusion for solar cell application. *J. Mater. Sci. Mater. Electron.* **27**, 13086–13092 (2016). <https://doi.org/10.1007/s10854-016-5452-y>
97. Kettle, J., Ding, Z., Horie, M., Smith, G.C.: XPS analysis of the chemical degradation of PTB7 polymers for organic photovoltaics. *Org. Electron.* **39**, 222–228 (2016). <https://doi.org/10.1016/j.orgel.2016.10.016>